FINAL TECHNICAL REPORT

REFINING THE SOUTHERN EXTENT OF THE 1872 OWENS VALLEY EARTHQUAKE RUPTURE – PALEOSEISMIC INVESTIGATIONS AT SAGE FLAT AND HAIWEE MEADOWS, CALIFORNIA

Recipient:
Fugro Consultants Inc., (formerly Fugro William Lettis & Associates, Inc.)
1777 Botelho Dr., Suite 262, Walnut Creek, CA 94596
(925) 256-6070; (925) 256-6076; URL www.fugroconsultants.com

Contributors:
Colin Amos[1], Andrew Lutz[2,*], Angela Jayko[3], Shannon Mahan[4], G. Burch Fisher[5], and Jeffrey Unruh[2,*,†]

[1]Department of Earth and Planetary Science, University of California, Berkeley
[2]Fugro Consultants, Inc., Walnut Creek, CA
[3]U.S. Geological Survey, U.C. White Mountain Research Station, Bishop, CA
[4]U.S. Geological Survey, Luminescence Dating Laboratory, Denver, CO
[5]Department of Earth Science, University of California, Santa Barbara

[*]currently: Lettis Consultants International, Inc.
[†]Principal Investigator

Program Elements I and III

Keywords:
Paleoseismology, neotectonics, lidar, eastern California shear zone, OSL dating

U. S. Geological Survey
National Earthquake Hazards Reduction Program
Award Number G09AP00133
Award Term August 31, 2009 to May 31, 2011

This research was supported by the U.S. Geological Survey (USGS), Department of the Interior, under USGS Award G09AP00133*. The views and conclusions contained in this document are those of the authors and should not be interpreted as necessarily representing the official policies, either expressed or implied, of the U.S. Government.*

Award Number G09AP00133
REFINING THE SOUTHERN EXTENT OF THE 1872 OWENS VALLEY EARTHQUAKE RUPTURE – PALEOSEISMIC INVESTIGATIONS AT SAGE FLAT AND HAIWEE MEADOWS, CALIFORNIA

C.B. Amos
Department of Earth & Planetary Science, 479A McCone Hall, University of California, Berkeley, CA, 94720
t: (510) 642-3993 f: (510) 643-9980
cbamos@seismo.berkeley.edu

A.T. Lutz
Lettis Consultants International, Inc., 1981 N. Broadway, Suite 330, Walnut Creek, CA 94596
t: (925) 482-0360 f: (925) 482-0361
lutz@lettisci.com

A.S. Jayko
U.S. Geological Survey, White Mountain Research Station, 3000 E. Line St. Bishop, CA
t. (760) 873-7040
ajayko@usgs.gov

S.A. Mahan
U.S. Geological Survey, Denver Federal Center, Box 25046 MS 974, 2nd and Center, Bldg. 15, Denver, CO 80225
t: (303) 236-7928 f: (303) 236-5556
smahan@usgs.gov

G.B. Fisher
Department of Earth Science, 1006 Webb Hall, University of California, Santa Barbara, CA, 93106
t: (805) 893-4499 f: (805) 893-2314
burch@eri.ucsb.edu

J.R. Unruh (PI)
Lettis Consultants International, Inc., 1981 N. Broadway, Suite 330, Walnut Creek, CA 94596
t: (925) 482-0360 f: (925) 482-0361
unruh@lettisci.com

ABSTRACT

Recent upward revision of the 1872 Owens Valley earthquake magnitude implies either additional, unrecognized rupture length or anomalously strong ground motions associated with this event. We investigate the first possibility through paleoseismic trenching south of the mapped surface rupture in the Haiwee area, where historical accounts indicate significant surface deformation immediately following the earthquake. Trenching focused on a prominent north-striking scarp, termed the Sage Flat fault, expressed in late Pleistocene alluvial fans east of Haiwee reservoir. Surficial mapping and ground-based lidar surveying suggest that this fault accommodates east-down normal motion, and possibly a similar amount of dextral slip. Trenching and luminescence dating reveal evidence for the most recent and penultimate surface ruptures at ca. 26 ka and before 30.1 ± 0.6 ka, respectively, and indicate a dip-slip-rate of ~0.1 mm/yr over this period. Although we discovered no evidence for recent surface rupture on the Sage Flat fault, a series of subvertical fractures and fissures cut across trench stratigraphy, consistent with secondary deformation associated with seismic shaking. As such, we suggest that possible ground disturbance in the Haiwee area during the 1872 event primarily reflected liquefaction-related deformation rather than triggered slip on faults. In addition, we suggest a structural and kinematic connection between the Owens Valley fault and dextral faults north of Lower Cactus Flat in the northwestern Coso Range. Consideration of these structures in the total extent of the Owens Valley fault suggests a length of 140 km, of which at least 113 km ruptured during the 1872 event.

TABLE OF CONTENTS

LIST OF TABLES

LIST OF FIGURES

1. INTRODUCTION

Source parameters for large historical earthquakes provide critical constraints on empirical relationships used in seismic hazard assessments (e.g., Wells and Coppersmith, 1994). Such assessments rely on both geological and seismological observations of past earthquakes to inform our understanding of the distribution and likelihood of future earthquake ruptures. In areas dominated by diffuse intracontinental shear, historical earthquakes also guide our expectations of the extent and size of surface ruptures that break multiple strands or fault segments in a single event. Two such events in eastern California, the 1992 Landers and 1872 Owens Valley earthquakes, produced relatively discontinuous surface ruptures that would arguably not have been identified beforehand as single through-going fault structures (Hough and Hutton, 2008). In each case, the complex and segmented nature of these surface ruptures reflects in some part a combination of relatively low average slip rates and long recurrence intervals for both faults (e.g., Bacon and Pezzopane, 2007; Rockwell et al., 2000). As such, geologic and seismologic observations of segmented surface ruptures provide key constraints on the hazards posed by large but infrequent earthquakes on faults away from major plate boundaries.

The recent and provocative suggestion that the 1872 Owens Valley earthquake magnitude be revised upwards to M_w 7.7-7.9 (cf. dePolo et al., 1991; Hough and Hutton, 2008) suggests that faults in the eastern California shear zone are capable of earthquake magnitudes rivaling the largest historical San Andreas events (cf. dePolo et al., 1991; Hanks and Kanamori, 1979) . Hough and Hutton's (2008) recent magnitude estimate relies on reinterpretation of macroseismic observations of shaking intensities during the 1872 event, which were more widely felt than the 1906 San Andreas earthquake. Given uncertainty in the total extent of the Owens Valley surface rupture, reflecting in part the segmented nature of the fault zone (Figure 1), Hough and Hutton (2008) explain this discrepancy by suggesting that 1) either the area of 1872 rupture was greater than currently recognized, or 2) the Owens Valley earthquake produced systematically higher ground motions over regional distances. Several historical accounts of surface deformation beyond the limits of the recognized 1872 rupture bolster the first possibility (e.g., Whitney, 1872a; 1872b). The second interpretation raises the important possibility that low slip-rate faults away from the San Andreas plate boundary might produce a fundamentally different class of earthquake, and importantly, that other such 100-140 km-long faults in California could be capable of similar large-magnitude events.

Here, we present the results from paleoseismic trenching at Sage Flat, south of the Owens Valley fault, to test whether the revised magnitude estimate (Hough and Hutton, 2008) can be attributed to additional surface rupture sough of the mapped fault trace (Figure 1). We completed three excavations across a fault scarp cutting upper Pleistocene alluvium near Haiwee Reservoir, where accounts by Whitney (1872a; 1872b) months after the earthquake suggest the presence of youthful scarps and substantial ground deformation. The trenched scarp, herein referred to as the

Sage Flat fault, traverses a relatively broad alluvial piedmont separating the northern Coso Range from the Sierra Nevada to the west (Figure 1). Although the roughly north-striking Sage Flat fault is discontinuous with the north-northwest trending Owens Valley fault, recent work in the area documents triggered slip during the 1872 earthquake on a similarly oriented fault cutting the northern Coso Range piedmont (Slemmons et al., 2008). Accordingly, we seek to document the timing of past earthquakes on the Sage Flat fault to test for triggered slip during the 1872 event. We also present new surficial geologic mapping, luminescence dating, and results from a ground-based lidar survey to constrain the orientation, timing, and slip rate on the Sage Flat fault. Our results limit the southwestern extent of the southern Owens Valley fault and place new constraints on the spatial extent of the 1872 surface rupture.

2. BACKGROUND AND PREVIOUS WORK

2.1 The Owens Valley Fault

The Owens Valley fault is part of a broad, distributed network of active strike-slip and normal faults east of the Sierra Nevada in California (Figure 1). Collectively termed the eastern California shear zone (Dokka and Travis, 1990) or Walker Lane belt (e.g., Stewart, 1988; Wesnousky, 2005), this zone of deformation accommodates roughly one quarter (9 ± 2 mm/yr) of the total dextral motion between the Pacific and North American plates (Bennett, 2003). Of the total displacement, the Owens Valley fault accounts for approximately 1 – 4.5 mm/yr of dextral slip (Beanland and Clark, 1994; Kirby et al., 2008; Lee et al., 2001; Bacon et al., 2003; Bacon and Pezzopane, 2007), averaged over the mid-to-late Pleistocene. Most estimates of fault slip-rate from geologic features fall at the lower end of that range, in broad agreement with rates derived from GPS data (Dixon et al., 2003).

The March 26, 1872 earthquake ruptured a distance of at least 113 km along the Owens Valley fault (Figure 1), from north of Big Pine to the southern shoreline of the now-dry Owens Lake playa (Slemmons et al., 2008). Although sparsely populated at the time, the earthquake caused approximately 27 fatalities in the nearby settlement of Lone Pine (Whitney, 1872a) and created strong ground motions felt over much of California (Oakshott et al., 1972; Stover and Coffman, 1992; Hough and Hutton, 2008). Initial field assessments of the damage extent and observations of surface deformation are presented by (Whitney 1872a; 1872b). Subsequent descriptions and observations in the following decades, including those by G.K. Gilbert in 1884, are summarized by Hough and Hutton (2008), Slemmons et al. (2008), and Beanland and Clark (1994). Nearly a century later, D.B. Slemmons, summarized in Hill (1972), carried out the first modern, systematic mapping of the Owens Valley fault and the 1872 rupture using low sun angle aerial photography. Carver (1969) also mapped the southern Owens Valley fault zone, focusing on deformation south of Diaz Lake around the margin of the Owens dry Lake. Notably, this work made the important distinction between surface deformation related to slip on faults and that

caused by shaking-induced lateral spreading and liquefaction, particularly focused around the late Pleistocene shorelines.

Subsequent published mapping of the Owens Valley fault documents the relatively complex surface trace of the 1872 rupture (Figure 1), which included slip on numerous secondary fault strands and subparallel to oblique fault splays (Slemmons, 1972; Beanland and Clark, 1994; Slemmons et al., 2008). These discontinuities suggest division of the fault into several fault segments or geometric sections based on the presence of fault stepovers, splays, or changes in the overall fault strike (Figure 1) (dePolo et al., 1991). Lateral offset from the 1872 surface rupture averaged 6 ± 2 m, although the maximum lateral offset (10 m) occurred at the southern end of the fault along one such strand immediately east of Lone Pine (Beanland and Clark, 1994). Compilation of fault offsets from the 1872 event along the length of the Owens Valley fault indicates that right-lateral offset dominated during the 1872 event, and occurred at an average ratio of 6:1 relative to subordinate east-down normal motion (Beanland and Clark, 1994).

Previous paleoseismic trench studies along the Owens Valley fault (Figure 1) reveal evidence for additional paleoearthquakes on segments that ruptured during the 1872 event. The penultimate event identified by Lee et al. (2001) near Big Pine occurred between 3 and 4 ka. Evidence for this earthquake is absent in fault trenches near Lone Pine, however, and Bacon and Pezzopane (2007) attribute this event to triggered slip caused by rupture on the nearby White Mountain frontal fault (Figure 1). The penultimate rupture identified by Bacon and Pezzopane (2007) near Lone Pine occurred between 8.8 – 10.2 ka, consistent with recurrence intervals estimated by Lubetkin and Clark (1988) and Bierman et al. (1995). Bacon and Pezzopane (2007) also provide evidence for an antepenultimate event sometime between 15 – 25 ka, yielding an average recurrence interval of roughly 10 k.y. or greater for the Owens Valley fault.

2.2 Extent of the 1872 earthquake rupture

Considerable uncertainty surrounds published estimates of the total length of the Owens Valley fault and the 1872 surface rupture. This uncertainty reflects a number of factors, including the discontinuous nature of surface faulting and complexities in the fault surface trace. Additionally, vagueness and variability in historical descriptions of surface deformation, in part due to confusion between surface faulting and fissures or liquefaction-related deformation caused by seismic shaking, confounds the true length of the surface rupture. The U.S. Geological Survey Quaternary fault and fold database (Bryant and Sawyer, 2002) lists the 1872 rupture section of the Owens Valley fault as spanning 118 km of a total 136 km fault length. This total length includes fault scarps north of Big Pine abutting the Sierra Nevada range front (Figure 1), extending north toward Bishop. Historical accounts from J.D. Whitney quoted and paraphrased in several sources (Bateman, 1961; Hobbs, 1910; Slemmons et al., 2008) suggest pervasive ground cracking between Bishop and Big Pine, although most studies limit the 1872 rupture termination immediately north of Big Pine (Beanland and Clark, 1994; Slemmons et al., 2008).

The southern shore of Owens dry lake represents the currently accepted southern termination of the Owens Valley fault and the 1872 surface rupture (Slemmons et al., 2008) (Figure 2). Offset historical shorelines identified by Slemmons, and later surveyed by Vittori et al. (1993) indicate 1.8 – 2.3 m of right-lateral offset during 1872 earthquake. Slemmons et al. (2008) also describe evidence for recent faulting south of the historical shoreline mapped by Carver (1969), including north-striking normal fault scarps flanking a series of low volcanic hills on the northern Coso piedmont (Red Ridge fault of Vittori et al., 1993, Figure 2). Inclusion of faulting at Red Ridge, presumably triggered during the 1872 earthquake, suggests a total rupture length of at least 113 – 120 km.

Several additional lines of evidence leave open the possibility of fault-related surface deformation south of the currently recognized 1872 rupture termination (Hough and Hutton, 2008). First, historical accounts from J.D. Whitney indicate pervasive ground cracking and differential settling in the vicinity of Haiwee Meadows, which coincides with the former spillway channel of Pleistocene Owens River (Bacon et al., 2006) now occupied by Haiwee Reservoir (Figure 2). Along the margin of Haiwee Meadows, Whitney (1972a) attributed a youthful scarp near Haiwee Creek, which drains into northern Rose Valley to the 1872 event. Although his description predates understanding of the specific connection between faulting and earthquakes, or the distinction between fault slip and lateral spreading, Whitney hints at a dependence of these features on groundwater and their position along the meadow:

> The dependence of the fissures upon the character of the soil was well exemplified at Haiwee Meadows, which occupy an oval area somewhat less than a mile in diameter, surrounded by hills, all around the border of which the soil is wet and heavy, owing to the presence of numerous springs in that position. Along this border the ground is broken by fissures, and the inside edge has settled as much as four or five feet. The hills to the east of the meadows are of volcanic sediment; and on visiting them a large crack was observed running in an easterly direction across one of the spurs, which looked fresh, as if it might have been made during the recent earthquake.

Indirect evidence for continuation of the 1872 surface rupture beyond its recognized boundaries comes from an apparent gap in microseismicity spanning the length of Owens Valley into the Haiwee area (Hough and Hutton, 2008). This gap also extends northward into the area where Whitney (1872a) described pervasive ground deformation associated with the 1872 earthquake. Although not conclusively linked with the 1872 surface rupture, Hough and Hutton (2008) note that overall low background rates of seismicity span an overall length of 140 km, similar to the total length of the Owens Valley fault.

To test whether or not surface faulting during the 1872 event extended onto structures near the former Haiwee Meadows, we completed an investigation of a previously unstudied fault at Sage Flat (Figure 2). This site was selected based on the prominent geomorphic expression of the Sage Flat fault in comparison with other nearby structures, and the locally steep scarp face, which implies a lesser degree of diffusion on this portion of the scarp. Additionally, the presence of finer-grained subsurface materials ponded against the Sage Flat fault provides a favorable target

for trenching relative to the coarse alluvium forming the surrounding bajada. In the following sections, we present additional background information and new constraints on Quaternary surface faulting in the Haiwee area and discuss potential kinematic and structural linkages with the Owens Valley fault.

3. STUDY AREA

3.1 Neotectonic Setting of the Haiwee Area, Southern Owens Valley

The Haiwee area lies in the southernmost Owens Valley (Figures 1 and 2) and occupies the north flank of a topographic divide that intermittently serves as a spillway between Pleistocene glacial lakes that occupy topographic lows in Owens and Rose Valleys. Incision of the Pleistocene Owens River channel through coalescing alluvial fans that underlie the divide attests to regional tectonic lowering of valley floors between Owens in the north and Searles Valley in the southeast. A buried structural step-up fault also likely contributes to the ~200 m topographic drop between Haiwee Reservoir and Rose Valley to the south (Figure 2).

Surface deformation east and northeast of the Sage Flat paleoseismic site records transfer of dextral shear from the Owens Valley fault system southward into the northern Coso Range via a series of small pull apart basins (e.g. Lower Cactus Flat, Figure 2) and horst blocks bounded by right-lateral strike-slip, normal, and oblique slip faults (Jayko, 2009). The extensional relay system continues to the south along the Coso Wash fault system and the dextral Little Lake and Airport Lake faults, which define an overall releasing stepover across the southern Coso Range (Unruh et al., 2002) (Figure 1). The Sage Flat paleoseismic site is also situated in a transitional zone between the normal or oblique Sierra Nevada Range front system to the south and the dextral Owens Valley fault zone (Figure 2).

Quaternary structures in the northwestern Coso Range east of Haiwee Reservoir include a series of discontinuous, north-northwest-striking normal and oblique normal faults, a broad tilt panel of west-dipping Plio-Quaternary cover sediments, and fault-related folds that deform clastic and volcanic deposits of the Plio-Pleistocene Coso Formation (Stinson, 1977; Duffield and Bacon, 1981; Jayko, 2009). Although no thoroughgoing structures directly connect to the Owens Valley fault to the north, several similarly oriented faults cut the surface of a Plio-Quaternary andesite (QTa, Figure 2) at the northern end of Lower Cactus Flat. These faults are identified in the mapping of Duffield and Bacon (1981), and Frankel et al. (2008) discuss evidence for dextral displacement along these structures. The easternmost of these faults is expressed as a series of alternately east and west-facing scarps and apparent shutter ridges that bound isolated pockets of Quaternary alluvium (Duffield and Bacon, 1981). Evidence for dextral displacement along the western fault strand is less well constrained (Duffield and Bacon 1981 map it as a normal fault), although we do note an apparent offset for both structures where they intersect the northern,

eroded contact between QTa and the underlying Coso Formation and basement rocks. To the south, both faults terminate into a series of northeast-striking, en-echelon normal faults bounding the western edge of Lower Cactus Flat (Jayko, 2009). Together, these faults represent the northern end of the extensional relay bounding the southern end of the Owens Valley fault zone.

Structures in the Haiwee area west of Lower Cactus Flat consist of a relatively discontinuous series of north-striking faults between the Sierra Nevada rangefront to the west and the Coso piedmont to the east (Figure 2). These faults display predominately east-down normal offsets and may accommodate some degree of westward tilting of the Haiwee block west of Lower Cactus Flat. The Sage Flat fault represents one of these east-down normal structures at the northern end of the Haiwee area.

3.2 Surficial Geology of Sage Flat

Sage Flat refers to the small, nearly closed depression southwest of the Owens Lake (Figure 2), where an isolated bedrock block interrupts the generally eastward flow of alluvial fans draining the steep eastern Sierra Nevada escarpment. Alluvial fans at Sage Flat are diverted around the southern tip of this block before merging with the east-sloping bajada at the southern end of Owens Valley. Across this bajada, several generations of Pleistocene and Holocene alluvial fans coalesce and are actively incised by small creeks and washes draining toward Haiwee Reservoir, which inundates the Pleistocene Owens River spillway channel (Bacon et al., 2006) and the former Haiwee Meadows (Figure 2). Surficial geologic mapping modified after Jayko (2009) suggests at least four generations of fan deposits at Sage Flat, including active alluvial washes (Figure 3). The eastward slope of older Pleistocene alluvial fans at Sage Flat is locally interrupted by a narrow zone of apparent westward tilting about an axis oriented parallel to the shore of Haiwee Reservoir (Figure 2). Younger fan deposits are graded to this low, where the modern valley axis is offset to the west from the former spillway channel to the east (Jayko, 2009).

Pleistocene alluvial fans at Sage Flat comprise boulders, cobbles, and sand sourced from steep mountainous catchments fringing the eastern Sierra escarpment (Figures 1 and 2). Construction of these fans reflects deposition of coarse debris-flow of materials onto the piedmont surface and subsequent incision and reworking during high runoff events (Whipple and Dunne, 1992). Incision and channelization isolates and stabilizes older fans as geomorphic surfaces, resulting in progressive formation of soil and desert pavement. Although numerical dates on fan surfaces at Sage Flat are unavailable, the relative degree of pavement and soil development provides clues as to the ages of these fan surfaces (Birkeland et al., 1991; Bull, 1991). We follow the mapping designations of Jayko (2009) and correlate older (Qfo), intermediate (Qfi), young (Qfy), and active (Qaw) fan surfaces with the early-to-mid Pleistocene, mid-to-late Pleistocene, late Pleistocene-to-Holocene, and Holocene-to-recent, respectively (Figure 3).

The study site at Sage Flat occupies a small, localized depression between coalescing lobes of young alluvial fans incised into older fan deposits (Figure 3). Compared to the surrounding terrain, this area is low enough to intersect the groundwater table, causing fine-grained spring deposits to accumulate along the base of the Sage Flat scarp. Saturation of alluvial materials west of the scarp also has resulted in the preservation of a patchy cover of eolian sand and silt capping older fan deposits on the upthrown side. As discussed in the following sections, these cover sediments may represent loess deposited during periods of Owens Lake desiccation in the Pleistocene.

3.3 Quaternary Faulting at Sage Flat

An arcuate, east-facing scarp traverses the Sage Flat piedmont for roughly 7 km, immediately south of the Owens dry lake (Figure 2). This scarp, informally termed the Sage Flat fault in this report, is one of several discontinuous north-striking faults expressed in Pleistocene alluvial fans west of Haiwee Reservoir. These faults are identified as cutting Quaternary alluvial materials in the regional geologic mapping of Stinson (1977) and Duffield and Bacon (1981). Subsequent detailed mapping of these structures by Wills (1989) and Jayko (2009) suggests that multiple generations of Pleistocene alluvial fans are cut by the Sage Flat fault, indicating multiple surface ruptures over this period. The tallest portion of the Sage Flat scarp (~8 m of local relief) is located at its northern end, prominently visible from Highway 395 to the east. Surficial mapping by Jayko (2009), however, indicates that the scarp in this location has been modified, either by fluvial erosion along the margin of a spillway channel, or by wave energy along a Pleistocene erosional shoreline of Owens Lake.

Detailed mapping of the Haiwee piedmont faults, termed the Haiwee section of the Sierra Nevada fault zone by Wills (1989), indicates subtle evidence for some component of right-lateral displacement in addition to east-down normal motion on these faults. In addition to laterally deflected drainages along range front faults farther south in Rose Valley (Figure 1), Wills (1989) suggested that the left-stepping, en echelon pattern of subtle, west-facing scarps just west of the Sage Flat fault (Figure 3) reflects an overall right-oblique sense of displacement. Field inspection of ephemeral channels crossing the Sage Flat fault (Figure 4) also reveals lateral deflection of these drainages on the order of 1 to 3 m, supporting the notion that this scarp accommodates some component of right-oblique normal motion.

The compound nature of the Sage Flat fault is well illustrated by terrestrial laser scanning (TLS) of offset alluvial fans at our trench site (Figure 5). This survey enables detailed topographic characterization of the scarp morphology and enables measurement of the total vertical offset across the fault. TLS surveying utilized a Riegl LMS-Z420i ground-based lidar system and resulted in collection of approximately 8.6 million individual laser returns at an average density of ~200 points/m^2. Non-ground returns from sparse brush covering the area were filtered using Bentley Microstation software, and the remaining returns were gridded to create a digital elevation model (DEM) at a nominal resolution of 50 cm (Figure 5) (cf. Perroy et al., 2010).

DEM elevations were extracted along the main trace of the Sage Flat scarp and ephemeral drainage channels in addition to a series of scarp-perpendicular topographic profiles (Figures 5 and 6). The greatest scarp relief occurs along the central portion of our site where older fan deposits (Qfo) to the west are upthrown 8 m relative to isolated buried older alluvial fan deposits and infilling younger fans (Qfy) to the east (Profiles E and F, Figure 6). The relatively steep scarp face in this location (locally ~30°) reflects in part the relatively cohesive nature of the underlying spring deposits and saturated eolian cover on the upthrown side. Localized collapse of the over-steepened scarp has occured on several subparallel east-facing scarps adjacent to our trench site (Figure 5). Young alluvial fan deposits are continuous across the Sage Flat scarp at the northern end of our TLS survey, where topographic profiling suggests 2.5 ± 0.3 m of vertical separation, corresponding to a normal, dip-slip displacement of ~2.6 m on a 75° dipping fault (Profile B, Figure 6). The margins of an ephemeral stream channel north of our survey (Figure 4a) show a similar magnitude of lateral deflection (~2 – 3 m) based on measurements made in the field (Figure 4).

4. PALEOSEISMIC TRENCHING AT SAGE FLAT

4.1 Site Conditions and Investigation Methods

Paleoseismic trenching of the Sage Flat fault was conducted in October 2010 to determine the timing and size of past surface ruptures, and to look for surface evidence of deformation associated with the 1872 Owens Valley earthquake. The trench site sits ~8 km south of Olancha, California near the intersection of Sage Flats Road and US-395. One ~20-m-long trench and two smaller, 7-m-long test pits were excavated in a localized depression roughly 350-m-wide (Figure 7a), bounded on the west by a locally 8-m-high east-facing fault scarp and on the north and south by the edges of incised alluvial fans (Figure 5).

Work at the Sage Flat site was performed under a land use permit issued by the Ridgecrest office of the Bureau of Land Management. The trench and test pits at the Sage Flat site were exposed using a track-mounted hydraulic excavator with a 36-in-wide bucket. The east wall of each excavation was scraped clean to remove bucket smear and polish from the trench exposures. A horizontal level datum was established, and stratigraphic contacts and other features (e.g., faults) were identified and flagged using nails and colored tape. The walls of the exposures were logged at 1 inch = 1 m to depict lithology, lithologic contacts between units and subunits, and pedogenic horizons. Scaled versions of our interpretive trench logs are presented in Figure 8, and detailed versions at the original draft scale are available as an electronic supplement (Plates S1 and S2).

Deposits exposed in the walls of the excavations were described using the Unified Soil Classification System (ASTM, 2000). Exposed stratigraphic units were distinguished primarily

based on variation in lithology, color, and relative soil profile development (e.g., color, consistency, and structure). Detailed soil profiles were described in each trench following Birkeland (1999) and Schoenberger et al. (2002). After completion of our study, the trench and test pits were backfilled using the original excavated materials, and the site was restored as closely as practical to original conditions.

4.2 Subsurface Geology

Subsurface materials exposed at the Sage Flat site can be grouped into three general categories, each separated by an unconformable contact: alluvial fan deposits (units 10 and 20), eolian sand (units 30, 32, 34, and 36), and scarp-derived colluvium (units 40, 50, 52, 54, 56, and 60) (Figure 7). Stratigraphic relationships between these units are shown in detailed logs for trench T1 and test pit TP1 (Figure 8). Shallow groundwater conditions limited the depth trench excavations to <2 m. Groundwater is also responsible for the pervasive weathering of uncovered subsurface deposits (Figure 7b), which obscured stratigraphic relationships and evidence for faulting in test pit TP2.

The lowest stratigraphic unit exposed at the Sage Flat site is fine- to coarse-grained sand containing gravel, cobbles, and boulders (unit 10). The western portion of this deposit is pervasively mottled with yellowish brown and dark greenish gray colors and contains abundant granitic cobbles and boulders that have weathered completely to grus. Stratification in unit 10 is indistinct due to the coarse nature of this deposit. A similar deposit (unit 20) rests stratigraphically above unit 10 at the eastern end of trench T1, and consists of yellowish brown fine- to medium-grained sand with silt and gravel, cobbles, and boulders. Unit 20 can be distinguished from unit 10 by a slightly finer-grained matrix and the presence of subhorizontal strings of flat-topped and weathered cobbles and boulders, possibly recording the former ground surface. The exact nature between units 10 and 20 is unclear, although weak evidence for faulting separates these two deposits at the base of trench T1. Both units 10 and 20 represent alluvial fan deposits correlated with the older alluvial fan surface (Qfo) surrounding the trench site (Figure 3).

The next oldest trench deposit, unit 30, is a light olive-brown silty clayey fine-grained sand unconformably overlying unit 10 at western end of trench T1 and test pit TP1 (Figure 8). Sand of unit 30 is unstratified and very well-sorted, suggesting eolian deposition as loess. The upper portion of unit 30 includes a soil profile with some carbonate accumulation (unit 32), weakly developed blocky structure (unit 34), and organic accumulation (unit 36). The basal contact with unit 10 is indistinct and irregular at the decimeter scale. Our trench logs depict this contact as subhorizontal and queried (Figure 8), although its irregularity may reflect obscuration by subsurface weathering due to saturated groundwater conditions.

The youngest stratigraphic deposits exposed in our trenches include two distinct packages of soil and scarp-derived colluvium (Figure 8). The oldest of these deposits, unit 40, consists of

unstratified brownish yellow silty fine- to medium-grained sand with gravel. Unit 40 is distinguished from the underlying alluvial fan gravels by a lighter color and increased silt component, although the basal contact between these deposits is somewhat gradational. Unit 40 contains cobbles and boulders of similar plutonic and metamorphic rocks as units 10 and 20. The overall geometry of this deposit defines an eastward-thickening wedge (Figure 8), presumably reflecting erosional stripping and local deposition at the top and bottom the scarp, respectively. Locally discontinuous soil horizons are present in unit 40. Unit 40 includes locally discontinuous soil horizons, possibly attributable to pre-depositional weathering of the former ground surface. The nature of the lower contact with eolian deposits of unit 30 is obscured by weathering and unclear, and is shown as queried on the trench logs (Figure 8).

Younger colluvial deposits of unit 50 unconformably overlie unit 40 and consist of yellow, fine- to medium-grained silty sand with gravel (Figure 8). The wedge-like geometry of this deposit similarly suggests deposition as scarp-derived colluvium. Unit 50 is easily distinguished from unit 40 by the general absence of cobbles and boulders and an increased silt component. Stratification within Unit 50 is defined by spring carbonate accumulation (units 52 and 54) and development of soil horizons (units 54 and 56), rather than grain-size sorting. Unit 52 consists of silty fine- to medium-grained sand and is thoroughly cemented with spring carbonate to form a continuous horizon up to 10 cm thick in trench T1 (Figure 8). The pedogenic horizon defining unit 52 bifurcates into numerous clay-lined seams that cross into other units, and is not exposed to the south in test pit TP1. Unit 54 is cemented with spring carbonate, similar to unit 52, but is less dense and features well-developed platy pedogenic structure. Unit 54 is poorly cemented and features subangular blocky pedogenic structure. The exact nature of the lower contact with unit 30 is unclear, but the relative abundance of sand and silt in Unit 50 is consistent with derivation from eolian deposits of unit 30.

The modern ground surface is underlain by unit 60, which consists of unstratified, medium- to coarse-grained sand with gravel (Figure 8). This deposit includes angular fragments of carbonate-cemented soil and sediment, representing active raveling of units 36 and 54 from the scarp face.

4.3 Faulting and Deformation

Excavations T1 and TP1 exposed a 3-to-4-m-wide zone of faulting midway along the Sage Flat scarp consisting of multiple steeply east-dipping to subvertical fault strands (Figures 8 and Plates S1 and S2). Despite extensive weathering and mottling driven by concentration of groundwater along the fault plane, detailed logging of fault exposures from both trenches T1 and TP1 consistently demonstrate the general characteristics and location of faulting at Sage Flat (Figure 8). In each trench, a prominent groundwater barrier along the western edge of the fault zone causes pervasive gley mottling at the upper, western end of the scarp, in contrast with brown and reddish hues of Mn- and Fe-oxide staining east of the fault (Figure 7b). Individual fault strands east of this barrier are less well-defined, but are visible as vertical strings of MnO-staining within

unit 10 overprinting weathered clay seams with poorly developed shear fabric (Figures 8 and Plates S1 and S2). These narrow zones coincide with abrupt vertical steps in the base of unit 40, although faults are indistinct where they continue upward into this colluvial unit. Younger colluvium of unit 50 is apparently undeformed across the Sage Flat fault and represents the oldest unfaulted stratigraphic unit (Figure 8). Where individual fault planes are visible in both trench walls, measured cross-trench fault orientations yield generally north-south to north-northeast fault strikes between approximately 355° and 030°.

No tilting, warping, or folding of individual stratigraphic layers is apparent in either trench exposure (Figure 8). The relatively coarse alluvial deposits at the base of each excavation, coupled with pervasive weathering within the fault zone, lend relatively large uncertainties to offset estimations from faulted stratigraphic horizons. Nonetheless, the total vertical separation of the base of colluvial unit 40 summed across individual fault strands in test pit TP1 and trench T1 totals approximately 0.8 to 1.4 m, respectively, though this is a minimum estimate that does not include displacement along minor fault strands west of the excavations (Figure 5). Based on the irregularity of the unconformity between this unit and the underlying alluvial gravels, we consider our tape-measurements of fault offset in each trench accurate within approximately 50 cm across the width of the fault zone. Total vertical offset of the Qfo fan surface at our trench site totals 7.5 ± 0.7 m, based on profiles extracted from our lidar survey (profile G, Figure 6). This vertical offset corresponds to a dip slip of roughly 7.8 m on a 75° fault plane similar to those exposed in our trenches (Figure 8). The absence of intact kinematic indicators in each trench or any continuous stratigraphic piercing lines between the two excavations precludes identification or measurement of the lateral component of displacement, if present.

A distinct set of subvertical fractures and carbonate, colluvial, and root-filled fissures cuts across stratigraphy at the eastern end of trench T1 (Figure 7c and 8). With the exception of the uppermost, loose colluvial soil of unit 60, these cracks penetrate each stratigraphic layer without measurable displacement. In places, these fissures cut across weathered boulders of alluvial unit 20 (Plate S1) and are continuous across the trench to the unlogged, northern wall. At their upper termination, these fissures are filled with loose colluvium and roots from the uppermost trench units (Figure 7c). Fissures and fractures appear disconnected and unrelated in their geometry to the adjacent fault planes (Figure 8), and possibly reflect deformation caused by seismic shaking.

5. OSL DATING

We used optically stimulated luminescence dating (OSL) in conjunction with the degree of soil profile development to constrain the depositional ages of stratigraphic units in the Sage Flat trenches. A total of six OSL tube-samples were collected from eolian unit 30 in trench T1 and colluvial units 40 and 54 in test pit TP1 (Figure 8). All OSL samples were prepared and analyzed using the single aliquot regeneration method on quartz at the U.S. Geological Survey

Luminescence Dating Laboratory in Denver, Colorado. Table 1 presents the luminescence dating results for each sample, and the detailed parameters and protocol for these OSL analyses are presented as supplementary materials (Tables S1 and S2). The OSL ages and the associated uncertainties are used to calculate the normal kernel density estimate, shown in Figure 9.

The validity of OSL ages depends upon sufficient exposure to sunlight prior to burial so that each sample is effectively reset to zero and the ages obtained date only the deposition interval of interest (Rhodes, 2011). As such, eolian deposits, such as those collected from the loess unit 30, represent ideal targets for OSL analysis. Although questions surround the suitability of coarse colluvium shed during scarp retreat events, OSL dating has proven effective in paleoseismic efforts to date finer-grained scarp colluvium or buried soil horizons (Forman et al. 2000; Heimsath et al., 2002; Hall and Goble, 2011). As such, we sampled the sandier portion of exposed colluvial wedge deposits, which represent reworked alluvium and loess that originally accumulated along the Sage Flat scarp. Radial plots were constructed for each sample in order to test for the effects of sediment mixing (i.e., bioturbation) or partial bleaching (i.e., incomplete exposure to sunlight prior to burial) as a bias toward younger or older ages, respectively (Figures S1 – S6).

OSL analysis yields late-Pleistocene ages for all samples from the Sage Flat trench exposures (Figure 9 and Table 1). With the exception of sample SFTP-6, these ages are broadly consistent with stratigraphic relationships revealed by our trench logging (Figure 8). The oldest measured OSL ages originate from colluvial unit 40, the buried and deformed colluvial wedge directly overlying alluvial fan gravels of unit 10 (Figure 8). Analysis of these two samples (SFTP1-3 and SFTP1-4) suggests ages of 29.7 ± 2.6 and 30.6 ± 1.2 ka, respectively (Table 1) and contribute to an older peak in the distribution centered at an average age of 30.1 ± 0.6 (1σ) (Figure 9). Although the radial plots associated with these ages indicate a significant partial bleaching component for sample SFTP1-4 (Figure S4), sample SFTP1-3 (Figure S3) indicates little bias toward older ages caused by non-reset quartz grains. As such, overall consistency between these two ages lends some credence to the relatively older peak age for these two samples.

OSL dates from the younger, undeformed colluvial wedge (unit 54, Figure 8) yield consistent ages of 26.2 ± 1.1 and 25.0 ± 1.0 ka for samples SFTP1-1 and 2, respectively (Table 1). These ages contribute to a younger, prominent peak in the composite density estimate (Figure 9) and correspond to an average age of 25.7 ± 0.9 ka (1σ). Although this peak overlaps at the 95% confidence limits with the older peak age from colluvial unit 40, radial plots for samples SFTP1-1 and 2 suggest only minor bias to either younger or older OSL ages (Figures S1 and S2).

Surprisingly, the two OSL ages calculated for samples collected from eolian sand at the top of trench T1 (unit 30, Figure 8) indicate relatively young and inconsistent ages. The older of these two dates (sample SFTP1-5) suggests a depositional age of 26.6 ± 1.5 ka, slightly older but in broad agreement with the younger colluvial wedge unit 54 (Table 1 and Figure 9). The radial plot for sample SFTP1-5 suggests some potential for bias in this age (Figure S5), although the

relatively finer-grained nature of colluvial unit 54 may suggest derivation from loess within unit 30. Younger ages calculated for sample SFT1-6 (20.3 ± 0.9 ka, Table 1) are outlying (Figure 9) and stratigraphically inconsistent with its location below the older sample SFTP1-5. The radial plot for sample SFT1-6 (Figure S6) provides no indication of bias in the calculated OSL age, although we note anomalously high levels of potassium, uranium, and thorium relative to other samples (Table 1), and thus the in-situ dosimetry might be a as a possible cause for this age inconsistency. As such, we favor the older of these two dates as representative of the depositional age of eolian unit 30 (26.6 ± 1.5 ka). Despite overlap between this age and the average for colluvial unit 54 (25.7 ± 0.9 ka), sample SFTP1-5 indicates that eolian unit 30 is slightly older than the young colluvium, consistent with our interpretation of the relatively obscured nature of this contact between these two units in our trenches (Figure 8).

Analysis of soil development in trench T1, though limited in ability to resolve absolute ages, is broadly consistent with the OSL dating results. The older colluvial unit 40 (Figure 8), though highly weathered from the presence of groundwater, contains very few distinct pedogenic features. An exception is a localized area of Bw-horizon development between stations 6.5 and 7.5 m (Plate S1), which may record colluvial reworking and pedogenesis of highly weathered unit 10 at the main fault scarp in the time period between deposition of units 40 and 54. Colluvial unit 50 exhibits discontinuous carbonate mottling, and units 54 and 56 are pervasively cemented by spring carbonate. Well-developed platy pedogenic structure characterizes colluvial unit 54, and unit 56 exhibits well-developed subangular blocky structure. This degree of soil development is consistent with a relatively prolonged period of pedogenesis (i.e., 25 ka), although the local addition of spring water and carbonate development precludes development of an age estimate based on relative weathering profiles from other landforms in the region.

6. DISCUSSION

6.1 Earthquake Chronology

Taken together, the results of paleoseismic trenching and OSL dating provide evidence for two late-Pleistocene surface rupturing earthquakes on the Sage Flat fault. Deposition of the younger colluvial unit 50 (Figure 8) resulted from scarp retreat closely following the most recent earthquake (MRE), which occurred prior to 25.7 ± 0.9 ka based on the average of two OSL ages (Figure 9). The younger colluvium of unit 50 contains a substantially higher percentage of finer-grained material than older colluvial deposits (Figure 8), which may reflect incorporation of loess stripped from eolian unit 30 at the top of the Sage Flat scarp. As such, the preferred OSL age from unit 30 (SFTP1-5, Table 1) provides a maximum constraint on the timing of the MRE at 26.6 ± 1.5 ka. This event disrupted the older colluvial wedge (unit 50, Figure 8), resulting in at least ~0.8 to 1.4 m of vertical separation of its basal contact with the underlying alluvial deposits. An additional, unknown component of lateral displacement may have occurred during this event,

causing right-lateral offset of streams inset within late Pleistocene fans immediately north of the trench site (Figure 5).

The penultimate surface-rupturing earthquake on the Sage Flat fault resulted in scarp retreat and formation of an older colluvial wedge (unit 50, Figure 8). Two OSL ages at the base of this contact provide a minimum age on this event of 30.1 ± 0.6 ka (Figure 9). Trench exposures at Sage Flat do not constrain the total amount of offset during this event, although we note the presence of a truncated shear zone at the eastern end of trench T1 juxtaposing alluvial deposits of unit 10 and 20 (Figure 8). This shear zone did not rupture during the MRE, but might be responsible for some of the total vertical separation of the Qfo surface (~7.5 m, Figure 6).

A number of subvertical fissures and fractures at the eastern end of trench T1 also imply some degree of surface deformation, possibly linked to seismic shaking on nearby faults. These features cut all stratigraphic units exposed in our trenches and locally include colluvial fill from the modern ground surface. Although no slip occurs along this fracture set, their apparently young age leaves open the possibility that they formed in response to strong ground motion during the 1872 Owens Valley earthquake. Linking these features to the 1872 event is purely conjectural, however, given the proximity of the Sage Flat site to numerous other Quaternary-active geologic structures capable of producing surface ruptures and seismic shaking (Figure 2).

6.2 New Fault Slip-Rate Constraints

The combined results of our lidar surveying and OSL dating provide constraints on the vertical slip-rate of the Sage Flat fault. If we assume that the penultimate earthquake on this fault produced a similar displacement to the MRE (~0.8 to 1.4 m), we can reasonably speculate that the ~2.5 m scarp cutting the Qfy surface north of the trench site (profile B, Figures 5 and 6) represents the product of 2 to 3 earthquakes. Given the minimum age on the penultimate earthquake here of ca. 30.1 ± 0.6 ka, this vertical separation translates into a maximum rate of dip slip of 0.09 ± 0.01 mm/yr, assuming a steeply dipping fault plane of ~75°. This calculation utilizes the Monte Carlo method for normal fault scarps outlined by Amos et al. (2010) and Rood et al. (2011). Although our lidar survey did not capture the laterally deflected stream inset within the young alluvial fan surface (Qfy) just north of profile B (Figure 4), field measurements indicate ~3 m of dextral offset. This estimate suggests the possibility of comparable magnitudes of both dextral and normal components of offset along the Sage Flat fault.

6.3 Implications for the Southern Owens Valley Fault Zone

Our paleoseismic study indicates that the 1872 Owens Valley earthquake did not produce triggered slip on the prominent scarp at Sage Flat. Despite its strong geomorphic expression, steep scarp face, and orientation similar to the Red Ridge fault (Figure 2), which accommodated triggered slip during the Owens Valley earthquake (Slemmons et al., 2008), our work suggests that the last surface-rupturing earthquake at Sage Flat occurred around ca. 26 ka (Figure 9). The

penultimate surface rupture on the Sage Flat fault occurred at least 4 k.y. earlier, sometime before 30.1 ± 0.6 ka. Although somewhat broadly constrained, the timing of the MRE does overlap with the antepenultimate (APE) earthquake identified for the Lone Pine strand of the Owens Valley fault at ca.15 to 25 ka (Bacon and Pezzopane, 2007; Lubetkin and Clark, 1988). Whether the MRE at Sage Flat occurred as triggered slip during this Owens Valley fault earthquake is unknown, however, given the relatively imprecise bounds on the timing of the APE Owens Valley event. In any case, given the pre-Holocene MRE at Sage Flat and the relatively long return period for Owens Valley earthquakes of ~10 k.y., (Bacon and Pezzopane, 2007), we consider the Sage Flat fault as a geomorphic analog for the pre-rupture state of Owens Valley fault segments prior to 1872. Viewing the Sage Flat fault in this context provides a somewhat unique perspective on the potential for large earthquake surface ruptures to occur on somewhat discontinuous fault segments without clear connection to structures with documented activity.

Trenching at Sage Flat uncovered evidence for recent fractures and subvertical fissures cutting across stratigraphy, including soil and colluvium at the top of the section underlying the modern ground surface (Figure 8). Although the exact age of these features is unknown, a possible origin could be as secondary, off-fault deformation caused by nearby seismic shaking. Again, interpreting these features as resulting from the 1872 earthquake is purely speculative, although the prevalence of secondary ground deformation in the Haiwee area might explain the original observations of surface disturbance by Whitney (1872a). We emphasize the point made by Hough and Hutton (2008) that Whitney's observations occurred before the geologic community made the specific connection between fault slip and earthquakes. Given the locally wet conditions at Sage Flat and presumably surrounding the former Haiwee Meadows, it seems plausible that surface deformation in this area reflects the secondary effects of seismic shaking (e.g., lateral spreading) rather than slip on faults. We also note that both Carver (1969) and Slemmons et al. (2008) describe abundant liquefaction-related surface deformation that occurred associated with the 1872 event within the saturated ground fringing Owens Lake.

The absence of evidence for recent triggered fault-slip at the Sage Flat paleoseismic site provides additional constraints on the southern boundary of the 1872 surface rupture. Although it is possible that such slip occurred on other faults in the Haiwee area that display Quaternary surface expression (Figure 2), the Sage Flat scarp represents the most prominent of these features (Figure 7a). As such, the extent of the 1872 rupture spanning from just north of Big Pine near Klondike Lake to the southern end of the Red Ridge fault totals at least 113 km (Slemmons et al., 2008) (Figure 1).

7. SUMMARY OF FINDINGS

Paleoseismic trenching at Sage Flat documents stratigraphic and geochronologic evidence for two late-Pleistocene surface-rupturing paleoearthquakes in the Haiwee area. Luminescence

dating of sand and silt from two distinct colluvial wedges and from loess deposits capping alluvial fan gravels suggests that the most recent and penultimate earthquakes at Sage Flat occurred at ca. 26 ka and prior to 30.1 ± 0.6 ka, respectively. The most recent event produced a minimum vertical displacement of 0.8 – 1.4 m. Trenched stratigraphy does not provide conclusive evidence for lateral offset, although dextral deflection of adjacent washes may suggest a comparable component of lateral displacement. Ground-based lidar surveying of deformed alluvial fans, in concert with OSL dating, indicates an average dip-slip-rate of ~0.1 mm/yr for the Sage Flat fault, albeit averaged over only 2 to 3 earthquakes.

Taken together, our results suggest that triggered slip did not occur on the Sage Flat fault during the 1872 Owens Valley earthquake. Instead, subvertical fissures and fractures cutting across trench stratigraphy may record secondary deformation associated with seismic shaking during this event. We do note, however, overlap between the timing of the most recent earthquake at Sage Flat and the antepenultimate Owens Valley fault earthquake at Lone Pine (ca. 15 – 25 ka, Bacon and Pezzopane, 2007). Although our trenching does not exclude the possibility of triggered surface rupture on other faults in the Haiwee area, we suspect that historical descriptions of surface deformation south of the recognized 1872 rupture (Whitney, 1872a) similarly reflect secondary or liquefaction related deformation (e.g., lateral spreads) rather than fault surface rupture. If true, our results limit the possible extension of the 1872 surface rupture into the area formerly occupied by Haiwee meadows.

Consideration of mapping by Duffield and Bacon (1981), Frankel et al. (2008), and Jayko (2009) suggests that discontinuous dextral, normal, and oblique faults north of Lower Cactus Flat provide a kinematic extension of the Owens Valley fault zone into the northwestern Coso Range. Although no thoroughgoing fault directly links these structures, apparent offset of the eroded margin of a Plio-Quaternary andesite is consistent with dextral displacement along faults north of Cactus Flat. Given the similarity between the orientation and sense of offset for these structures and the Owens Valley fault, we suggest addition to the overall fault length, totaling approximately 140 km from south of Bishop to Lower Cactus Flat. Late Quaternary alluvial deposits in Lower Cactus Flat do not preserve clear evidence for rupture during the 1872 event, limiting the southern endpoint of the earthquake surface rupture to the Red Ridge fault (Slemmons et al., 2008). From north of Big Pine to Red Ridge, this surface rupture spans roughly 113 km of the total 140-km-long Owens Valley fault.

Exclusion of possible surface faulting at the Sage Flat paleoseismic site associated with the 1872 earthquake confirms that this event ruptured with a relatively high surface displacement (6 ± 2 m, Beanland and Clark, 1992) relative to its length (Hough and Hutton, 2008). Similar displacements were produced during the 1857 and 1906 San Andreas events (e.g., Sieh, 1978) along fault sections two to three times longer than the Owens Valley trace. This result supports the idea that earthquakes along discontinuous, low slip-rate fault systems that characterize areas of diffuse intracontinental shear (e.g., the eastern California shear zone) might produce stronger ground motions than long-lived, plate-boundary (e.g., San Andreas) structures. Given the

relatively long return periods for earthquakes like the Owens Valley event (ca. 10 k.y., Bacon and Pezzopane, 2007), many such faults are understudied and pose an unknown amount of seismic hazard. Although complete evaluation of this hypothesis is beyond the scope of our paper, we note that scarps like the Sage Flat fault might serve as an analog for the pre-rupture state of the Owens Valley fault system. Additional work on this question should focus on the physical basis for anomalously strong ground motions associated with intraplate earthquakes and field documentation of multi-segment fault surface ruptures in similar tectonic environments.

8. ACKNOWLEDGEMENTS

We gratefully acknowledge Seth Dee for processing and analyzing luminescence samples. We heartily thank Paul Hancock, Anita McProud, and Katherine Hancock of Lone Pine, CA for logistical support during our trenching. Bodo Bookhagen kindly provided use of TLS survey equipment. Keith Kelson provided trench review, and Doug Clair construction of Bishop, CA performed the excavation and backfilling of our trenches. We acknowledge the Bureau of Land Management in Ridgecrest, CA for facilitating the permit processes. Thanks also to students of the Dartmouth geology STRETCH program for their insight and curiosity during their visit to our trenches.

9. REPORTS/ABSTRACTS PUBLISHED

This report has been submitted for peer review and eventual publication to the *Bulletin of the Seismological Society of America* as:

Amos, C.B., A.T. Lutz, A.S. Jayko, S.A. Mahan, G.B. Fisher, and J.R. Unruh, 2012, Refining the southern extent of the 1872 Owens Valley Earthquake rupture: Paleoseismic investigations in the Haiwee area, southeastern California, submitted to the *Bulletin of the Seismological Society of America.*

10. REFERENCES

Amos, C. B., Kelson, K. I., Rood, D. H., Simpson, D. T., and Rose, R. S., 2010, Late Quaternary slip rate on the Kern Canyon fault at Soda Spring, Tulare County, California: Lithosphere, v. 2, no. 6, p. 411-417.

ASTM (American Society for Testing and Materials), 2000. United Soil Classification System (USCS) visual manual method. ASTM manual 2488-93.

Bacon, S. N., Burke, R. M., Pezzopane, S. K., and Jayko, A. S., 2006, Last glacial maximum and Holocene lake levels of Owens Lake, eastern California, USA: Quaternary Science Reviews, v. 25, no. 11-12, p. 1264-1282.

Bacon, S. N., and Pezzopane, S. K., 2007, A 25,000-year record of earthquakes on the Owens Valley fault near Lone Pine, California: Implications for recurrence intervals, slip rates, and segmentation models: Geological Society of America Bulletin, v. 119, no. 7-8, p. 823-847.

Bacon, S. N., Pezzopane, S. K., and Burke, R. M., 2003, Paleoseismology on the Owens Valley fault and Latest Quaternary stratigraphy in Owens Valley near Lone Pine, eastern California, Final Technical Report, National Earthquake Hazard Reduction Program awards 01-HQ-GR-0013 and 02-HQ-GR-0003.

Bateman, P. C., 1961, Willard D. Johnson and the strike-slip component of fault movement in the Owens Valley, California, earthquake of 1872: Bulletin of the Seismological Society of America, v. 51, no. 4, p. 483-493.

Beanland, S., and Clark, M. M., 1994, The Owens Valley fault zone, eastern California, and surface faulting associated with the 1872 earthquake, U.S. Geological Survey Bulletin 1982, 32 p.

Bennett, R. A., Wernicke, B. P., Niemi, N. A., Friedrich, A. M., and Davis, J. L., 2003, Contemporary strain rates in the northern Basin and Range province from GPS data: Tectonics, v. 22, no. 2.

Bierman, P. R., Gillespie, A. R., and Caffee, M. W., 1995, Cosmogenic ages for earthquake recurrence intervals and debris flow fan deposition, Owens-Valley, California: Science, v. 270, no. 5235, p. 447-450.

Birkeland, P. W., 1999, Soils and Geomorphology, 3rd ed., New York, Oxford University Press, 372 p.

Birkeland, P. W., Machette, M. N., and Haller, K., 1991, Soils as a tool for applied Quaternary geology, Utah Department of Natural Resources, Geological and Mineral Survey Miscellaneous Publication, 63 p.

Brossy, C. C., Kelson, K.I., Amos, C.B., Baldwin, J.N., Kozlowicz, B., Simpson, D., Ticci, M.G., Lutz, A.T., Kozaci, O., Streig, A., Turner, R., and Rose, R, 2012, Map of the late Quaternary active Kern Canyon and Breckenridge faults, Southern Sierra Nevada, California: Geosphere.

Bryant, W. A., and Sawyer, T. L., 2002, Fault number 51b, Owens Valley fault zone, 1872 rupture section, Quaternary fault and fold database of the United States, U.S. Geological Survey.

Bull, W. B., 1991, Geomorphic responses to climatic change, New York, NY, Oxford University Press, 326 p.

Carver, G. A., 1969, Quaternary Tectonism and Surface Faulting in the Owens Lake Basin, California, MSc. thesis: University of Nevada, Reno, 113 p.

dePolo, C. M., Clark, D. G., Slemmons, D. B., and Ramelli, A. R., 1991, Historical surface faulting in the Basin and Range Province, Western North-America - Implications for fault segmentation: Journal of Structural Geology, v. 13, no. 2, p. 123-136.

Dixon, T. H., Norabuena, E., and Hotaling, L., 2003, Paleoseismology and Global Positioning System: Earthquake-cycle effects and geodetic versus geologic fault slip rates in the Eastern California shear zone: Geology, v. 31, no. 1, p. 55-58.

Dokka, R. K., and Travis, C. J., 1990, Role of the Eastern California shear zone in accommodating Pacific-North-American plate motion: Geophysical Research Letters, v. 17, no. 9, p. 1323-1326.

Duffield, W. A., and Bacon, C. R., 1981, Geologic map of the Coco volcanic field and adjacent areas, Inyo County, California, scale 1:50,000.

Frankel, K. L., Glazner, A. F., Kirby, E., Monastero, F. C., Strane, M. D., Oskin, M. E., Unruh, J. R., Walker, J. D., Anandakrishnan, S., Bartley, J. M., Coleman, D. S., Dolan, J. F., Finkel, R. C., Greene, D., Kylander-Clark, A., Marrero, S., Owen, L. A., and Phillips, F., 2008, Active tectonics of the eastern California shear zone: Field Guides, v. 11, p. 43-81.

Hall, S., and Goble, R., 2011, New optical ages of the Mescalero sand sheet, southeastern New Mexico: New Mexico Geology, v. 33, no. 1, p. 9-16.

Hanks, T. C., and Kanamori, H., 1979, Moment magnitude scale: Journal of Geophysical Research, v. 84, no. NB5, p. 2348-2350.

Heimsath, A. M., Chappell, J., Spooner, N. A., and Questiaux, D. G., 2002, Creeping soil: Geology, v. 30, no. 2, p. 111-114.

Hill, M. R., 1972, A centennial... The great Owens Valley earthquake of 1972: California Geology, v. 25, p. 51-54.

Hobbs, W. H., 1910, The earthquake of 1872 in the Owens Valley, California: Beit. Geophys., v.

10, p. 352-385.

Hough, S. E., and Hutton, K., 2008, Revisiting the 1872 Owens Valley, California, earthquake: Bulletin of the Seismological Society of America, v. 98, no. 2, p. 931-949.

Jayko, A. S., 2009, Surficial geologic map of the Darwin Hills 30' x 60' quadrangle, Inyo County, California, scale 1:100,000.

Kirby, E., Anandakrishnan, S., Phillips, F., and Marrero, S., 2008, Late pleistocene slip rate along the Owens Valley fault, eastern California: Geophysical Research Letters, v. 35, no. 1.

Lee, J., Spencer, J., and Owen, L., 2001, Holocene slip rates along the Owens Valley Fault, California: Implications for the recent evolution of the Eastern California Shear Zone: Geology, v. 29, no. 9, p. 819-822.

Lubetkin, L. K. C., and Clark, M. M., 1988, Late Quaternary activity along the Lone Pine fault, eastern California: Geological Society of America Bulletin, v. 100, no. 5, p. 755-766.

Oakeshott, G. B., Greensfelder, R. W., and Kahle, J. E., 1972, 1872: one hundred years later: California Geology, v. 25, p. 55-62.

Perroy, R. L., Bookhagen, B., Asner, G. P., and Chadwick, O. A., 2010, Comparison of gully erosion estimates using airborne and ground-based LiDAR on Santa Cruz Island, California: Geomorphology, v. 118, no. 3-4, p. 288-300.

Prescott, J. R., and Hutton, J. T., 1994, Cosmic-Ray Contributions to Dose-Rates for Luminescence and Esr Dating - Large Depths and Long-Term Time Variations: Radiation Measurements, v. 23, no. 2-3, p. 497-500.

Rhodes, E. J., 2011, Optically Stimulated Luminescence Dating of Sediments over the Past 200,000 Years: Annual Review of Earth and Planetary Sciences, v. 39, no. 1, p. 461-488.

Rockwell, T. K., Lindvall, S., Herzberg, M., Murbach, D., Dawson, T., and Berger, G., 2000, Paleoseismology of the Johnson Valley, Kickapoo, and Homestead Valley faults: Clustering of earthquakes in the eastern California shear zone: Bulletin of the Seismological Society of America, v. 90, no. 5, p. 1200-1236.

Rood, D. H., Burbank, D. W., and Finkel, R. C., 2011, Spatiotemporal patterns of fault slip rates across the Central Sierra Nevada frontal fault zone: Earth and Planetary Science Letters, v. 301, no. 3-4, p. 457-468.

Schoenberger, P. J., Wysocki, D.A., Benham, E.C., and Broderson, W.D, 2002, Field book for describing and sampling soils: Version 2.0, Lincoln, Nebraska, Natural Resources

Conservation Service, National Soil Survey Center.

Sieh, K. E., 1978, Slip Along San-Andreas Fault Associated with Great 1857 Earthquake: Bulletin of the Seismological Society of America, v. 68, no. 5, p. 1421-1448.

Slemmons, D.B, Vittori, E., Jayko, A.S., Carver, G.A., and Bacon, S.N., 2008, Quaternary Fault and Lineament Map of Owens Valley, Inyo County, Eastern California: Geological Society of America Map and Chart Series 96, 25 pp. 2 sheets, scale:1:100,000, doi:10.1130/2008.MCH096.

Stewart, J. H., 1988, Tectonics of the Walker Lane Belt, western Great Basin Mesozoic and Cenozoic deformation in a zone of shear, *in* Ernst, W. G., ed., Metamorphism and Crustal Evolution of the Western US, Ruby Volume VII: Englewood Cliffs, NJ, Prentice Hall, p. 685-713.

Stinson, M.C., 1977, Geology of the Haiwee Reservoir 15' Quadrangle, Inyo County, California: California Division of Mines and Geology Map Sheet 37, scale 1:62,500.

Stover, C. W., and Coffman, J. L., 1992, Seismicity of the United States 1568-1989 (Revised), U.S. Geological Survey Professional Paper 1527.

Unruh, J. R., Hauksson, E., Monastero, F. C., Twiss, R. J., and Lewis, J. C., 2002, Seismotectonics of the Coso Range-Indian Wells Valley region, California: Transtensional deformation along the southeastern margin of the Sierran microplate, *in* Glazner, A. F., Walker, J. D., and Bartley, J. M., eds., Geologic Evolution of the Mojave Desert and Southwestern Basin and Range: Geologial Society of America Memoir, Volume 195, p. 277-294.

Vittori, E., Michetti, A. M., Slemmons, D. B., and Carver, G., 1993, Style of recent surface deformation at the south end of the Owens Valley fault zone, eastern California, Geological Society of America Abstracts with Programs, v. 5, p. 159.

Wells, D. L., and Coppersmith, K. J., 1994, New empirical relationships among magnitude, rupture length, rupture width, rupture area, and surface displacement.: Bulletin of the Seismological Society of America, v. 84, p. 974-1002.

Wesnousky, S. G., 2005, Active faulting in the Walker Lane: Tectonics, v. 24, no. 3.

Whitney, J. D., 1872a, The Owens Valley earthquake, part I: Overland Monthly, v. 9, p. 130-140.

Whitney, J. D., 1872b, The Owens Valley earthquake, part II: Overland Monthly, v. 9, p. 266-278.

Wills, C.J., 1989, Sierra Nevada fault zone – Haiwee segment, Inyo County, California: California Division of Mines and Geology Fault Evaluation Report FER-208, 6 p.

Table 1. Results of Optically Stimulated Luminescence Analyses for Sage Flat

Sample ID, Location	% Water content[a]	K (%)[b]	U (ppm)[b]	Th (ppm)[b]	Cosmic dose additions (Gy/ka)[c]	Total Dose Rate (Gy/ka)	Equivalent Dose (Gy)	n[d]	Age (ka)[e]
SFTP1-1 (TP-1, Unit 54)	15 (38)	1.52 ± 0.02	1.84 ± 0.06	5.80 ± 0.22	0.23 ± 0.02	2.28 ± 0.05	59.9 ± 2.16	17 (20)	26.3 ± 11.1
SFTP1-2 (TP-1, Unit 54)	14 (50)	1.49 ± 0.02	1.71 ± 0.06	6.90 ± 0.21	0.24 ± 0.02	2.21 ± 0.04	55.3 ± 1.94	22 (25)	25.0 ± 1.0
SFTP1-3 (TP-1, Unit 40)	13 (59)	1.48 ± 0.02	2.15 ± 0.06	7.33 ± 0.23	0.23 ± 0.02	2.21 ± 0.04	65.6 ± 5.51	17 (20)	29.7 ± 2.6
SFTP1-4 (TP-1, Unit 40)	20 (35)	1.40 ± 0.02	1.17 ± 0.05	4.32 ± 0.08	0.23 ± 0.02	1.64 ± 0.02	50.1 ± 1.85	23 (25)	30.6 ± 1.2
SFT1-5 (T-1, Unit 30)	20 (44)	1.43 ± 0.02	2.05 ± 0.07	6.91 ± 0.20	0.22 ± 0.02	2.43 ± 0.04	64.6 ± 3.42	17 (20)	26.6 ± 1.5
SFT1-6 (T-1, Unit 30)	22 (40)	2.39 ± 0.04	2.48 ± 0.08	11.4 ± 0.35	0.19 ± 0.01	3.67 ± 0.07	74.5 ± 2.76	19 (20)	20.3 ± 0.9

[a] Field moisture, figures in parentheses indicate complete saturation %. Ages calculated using about 25% saturation for Holocene aged samples and 40% saturation for Pleistocene aged samples.

[b] Analyses obtained using laboratory Gamma Spectrometry (high resolution Ge detector) and readings are delayed after 21 days of being sealed in the planchet (used for dose rates).

[c] Cosmic doses and attenuation with depth were calculated using the methods of Prescott and Hutton (1994). See supplementary material for details.

[d] Number of replicated equivalent dose (De) estimates used to calculate the mean. Figures in parentheses indicate total number of measurements made including failed runs with unusable data.

[e] Dose rate and age for fine-grained 180-90 microns quartz sand. Linear + exponential fit used on equivalent dose, errors to one sigma.

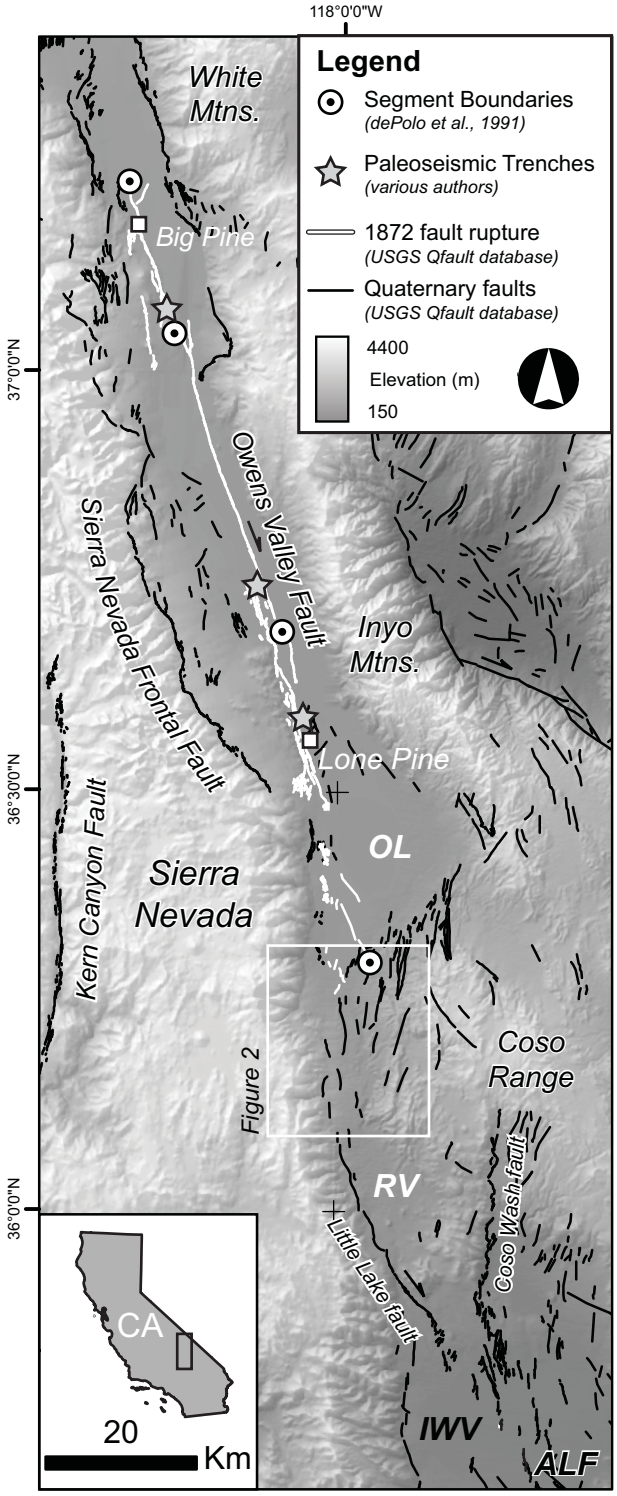

Figure 1. Regional overview of the Owens Valley fault and the 1872 earthquake surface rupture, showing the location of previous paleoseismic trenches and fault section boundaries from dePolo et al. (1991). Fault traces are taken from the U.S. Geological Survey's Quaternary fault and fold database (Bryant and Sawyer, 2002) with the exception of the Kern Canyon fault (Brossy et al., 2012). ALF – Airport Lake fault, OL – Owens Lake, RV – Rose Valley, IWV – Indian Wells Valley

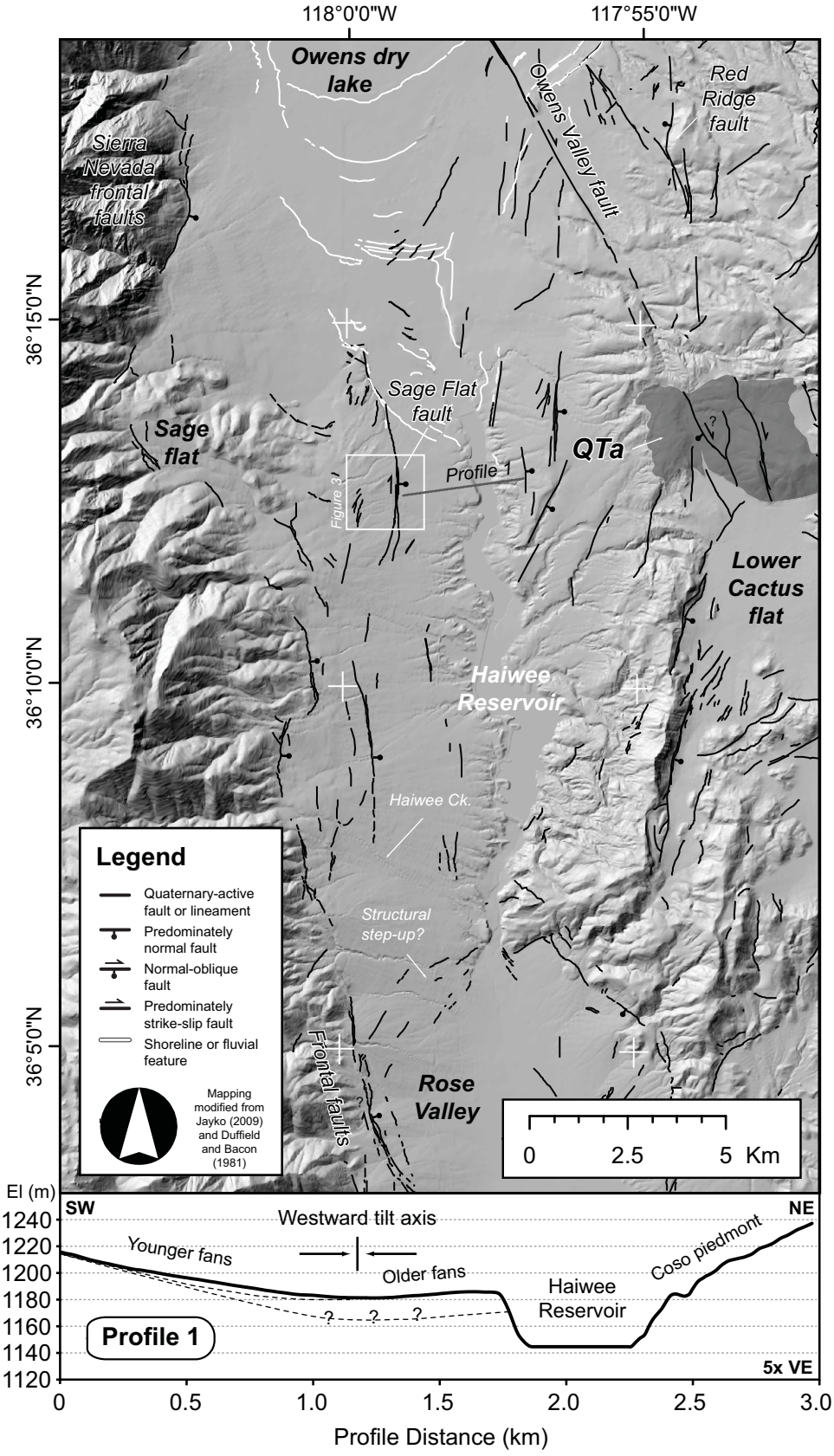

Figure 2. Hillshade image showing the Sage Flat fault and other Quaternary active structures in the Haiwee area. Fault mapping is modified after Jayko (2009). QTa refers to a Plio-Quaternary andesite flow (Duffield and Bacon, 1981) cut by a series of faults along strike of the Owens Valley fault. Inset shows a topographic profile extracted from the NED 10-m digital topography across the Sage Flat piedmont and Haiwee Reservoir.

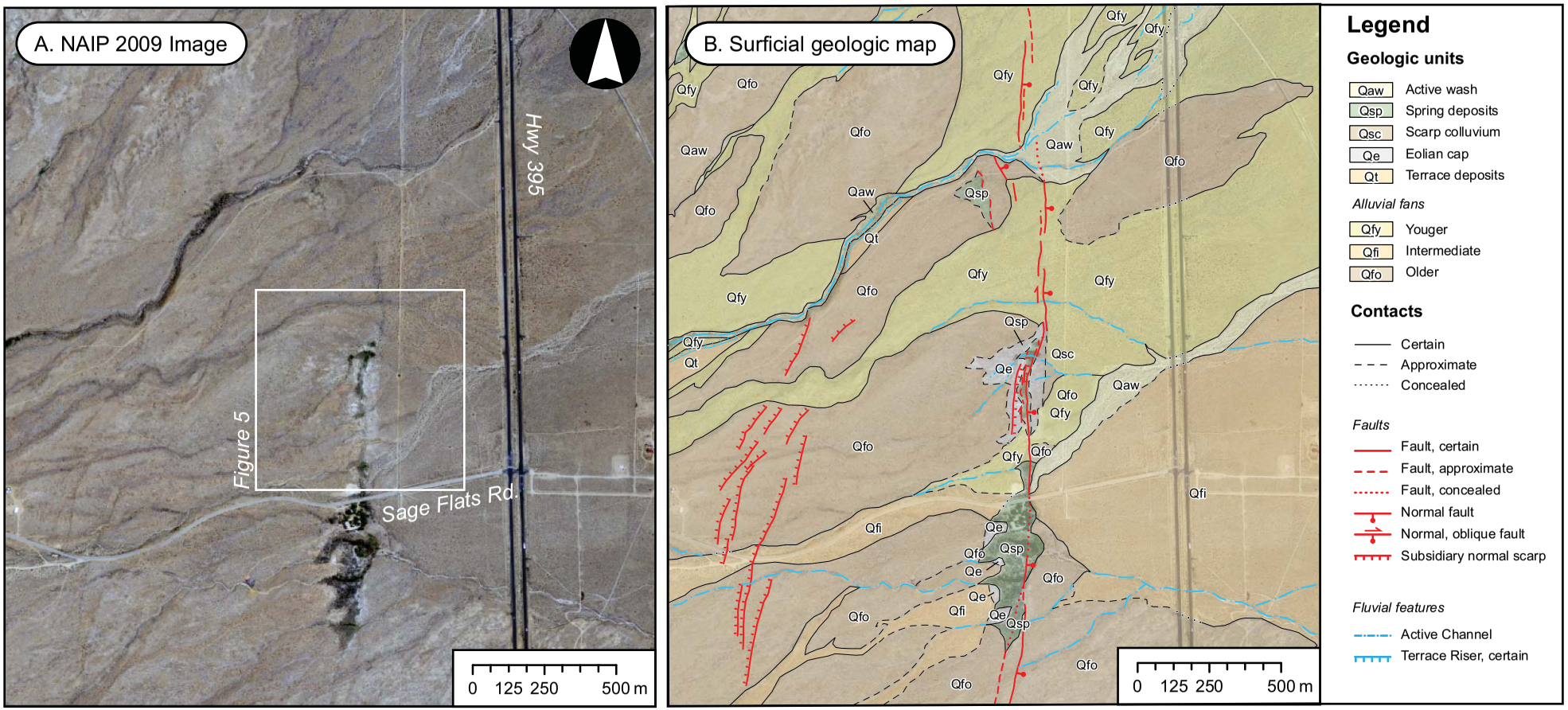

Figure 3. A) 2009 NAIP image showing the Sage Flat site. B) Surficial geologic map of the Sage Flat trench site, modified after Jayko (2009).

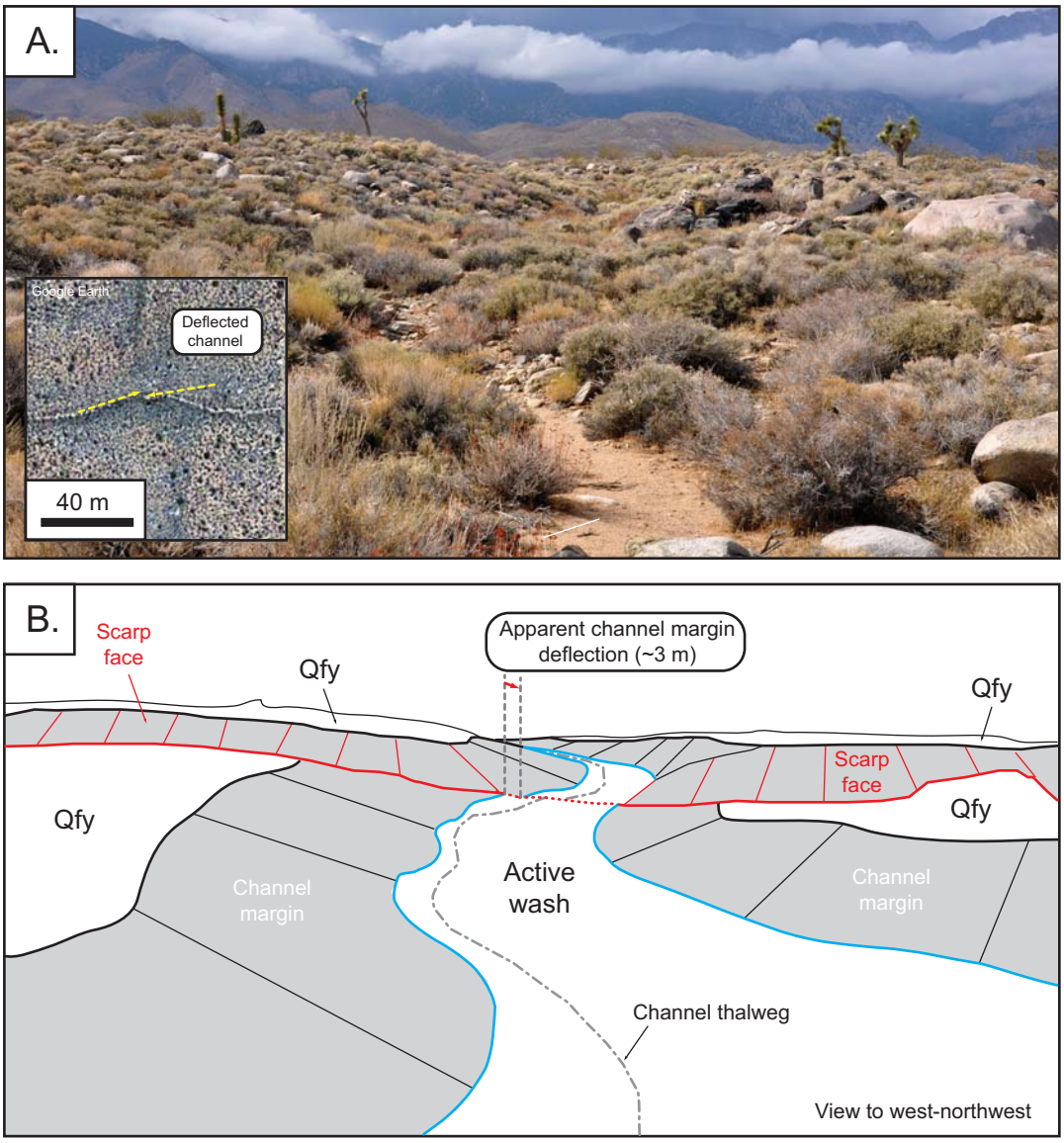

Figure 4. A) Field photograph and B) schematic line drawing of the Sage Flat scarp and the laterally deflected margins of an ephemeral wash intersecting the fault. Joshua trees on the scarp are ~2 m tall. Location of this vantage is shown in Figure 5. Inset in A) shows 2009 NAIP aerial imagery of the offset channel.

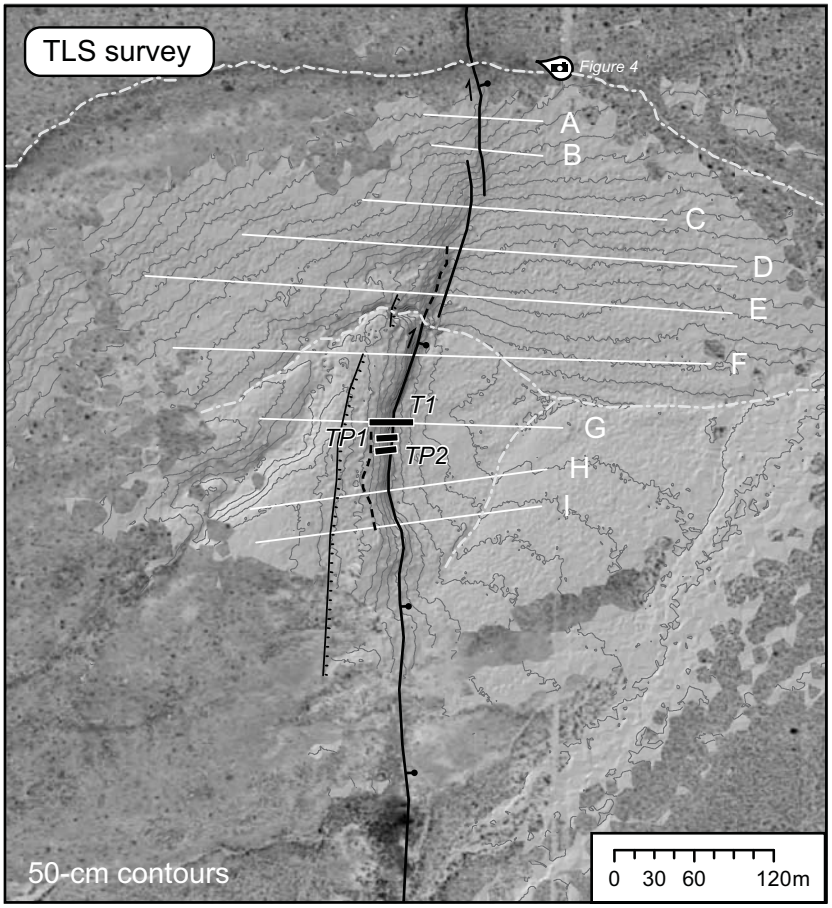

Figure 5. Hillshade image of the Sage Flat trench site created from 50-cm-resolution digital topography surveyed using a ground-based lidar. White lines correspond to the location of profiles shown in Figure 6.

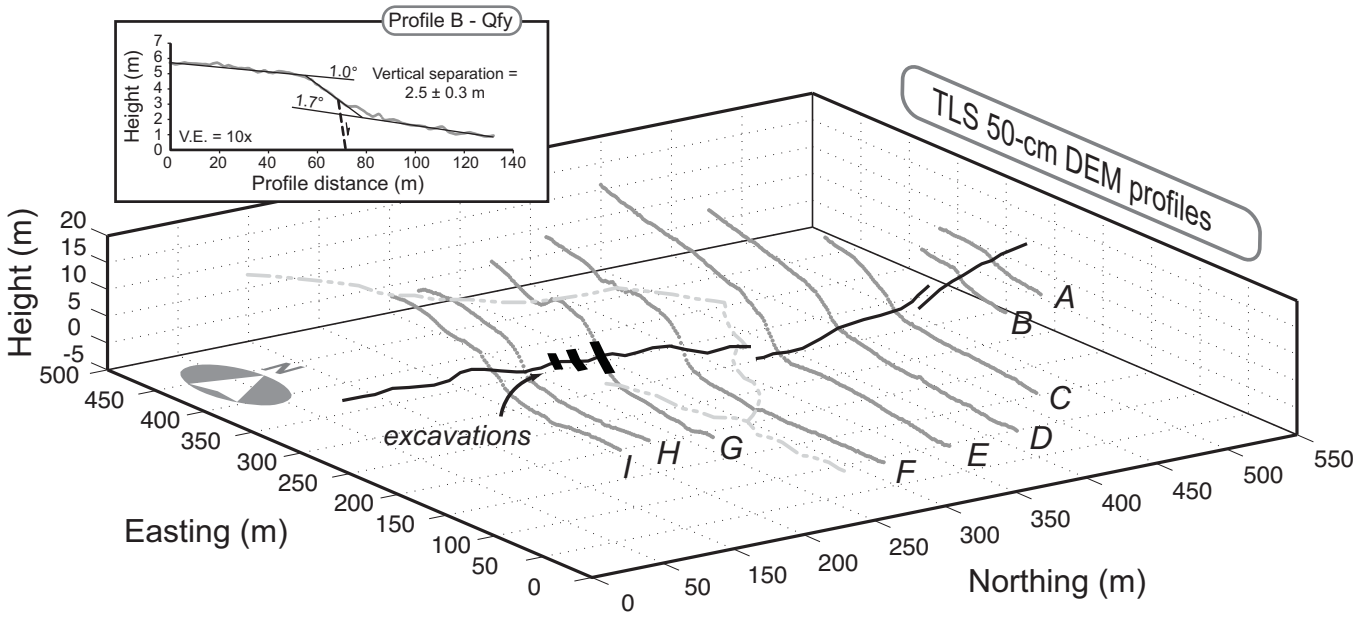

Figure 6. 3D-perspective image of topographic profiles extracted from our lidar survey. Scarp-normal profiles (gray) show the compound nature of the Sage Flat scarp, while profiles along the fault (black) and transverse ephemeral washes (dashed line) show apparent dextral deflections where they cross the scarp. Inset shows detail of Profile B across the Qfy surface north of our trench site.

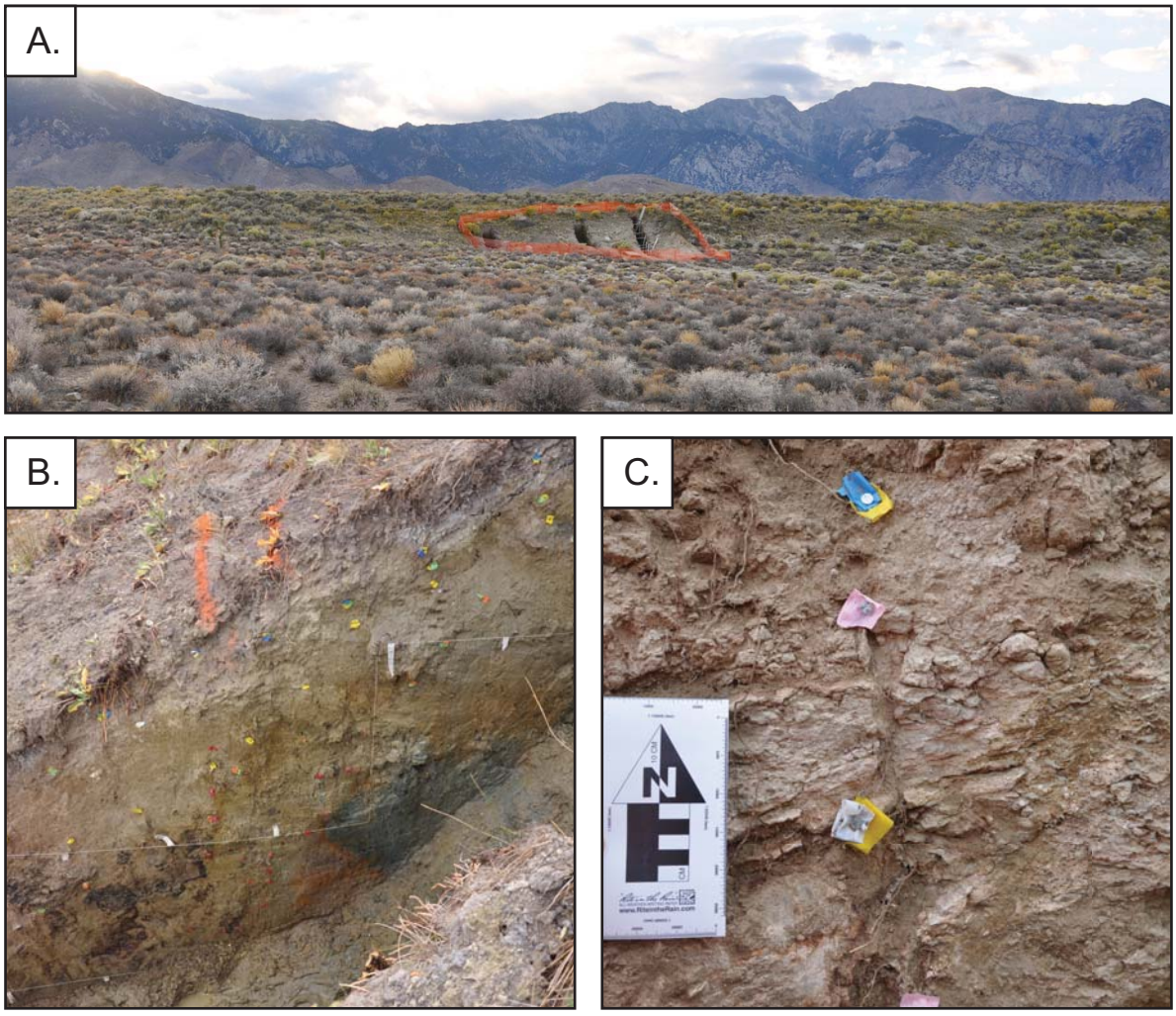

Figure 7. Field photographs of A) excavations at the Sage Flat site, looking northwest, B) the southern wall of test pit TP1, and C) a close up of subvertical fissures filled by young roots and colluvium at the eastern edge of trench T1.

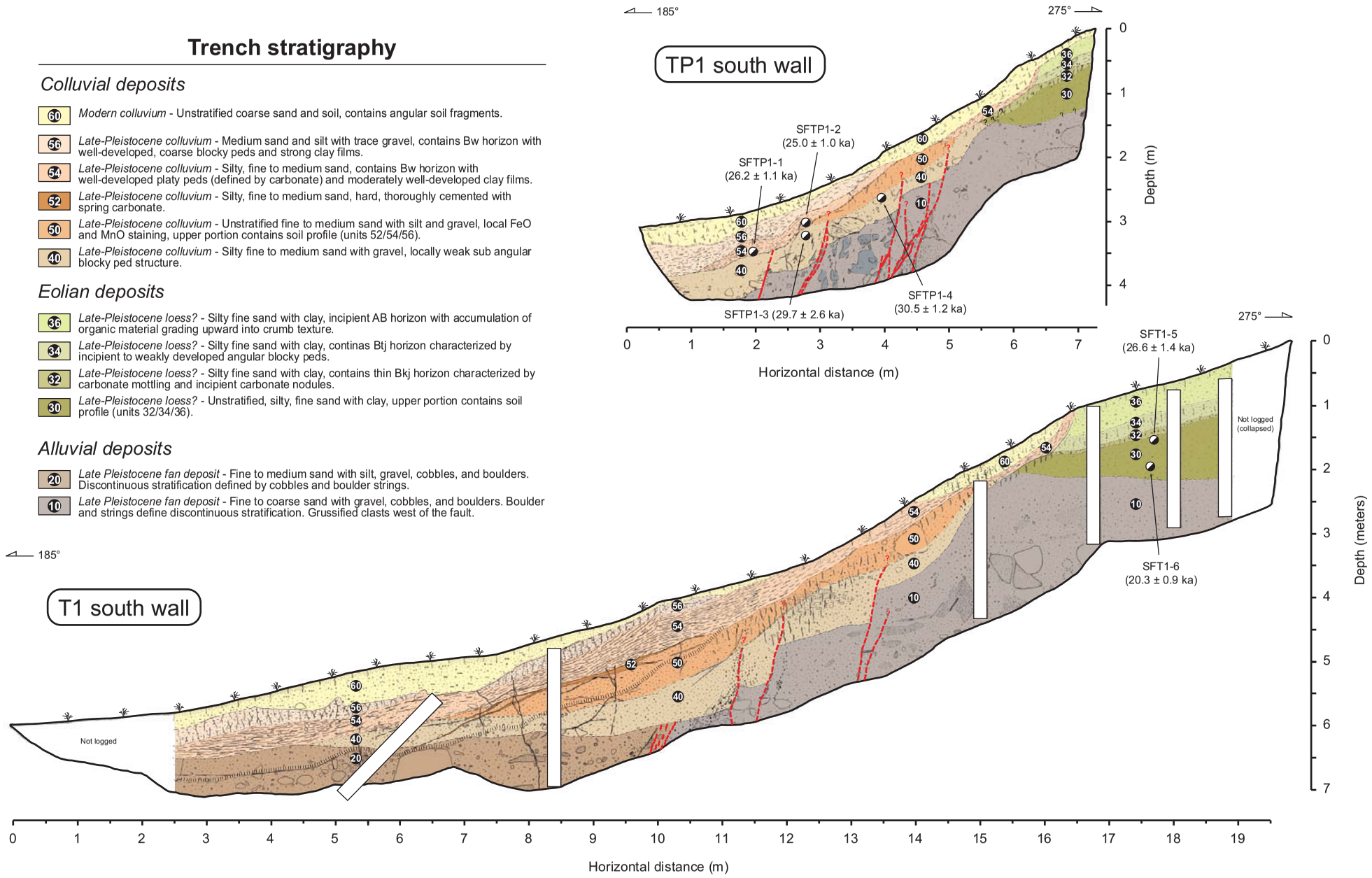

Figure 8. Scaled versions of our interpretive trench logs across the Sage Flat fault. Detailed versions at the original scale are presented as supplementary materials.

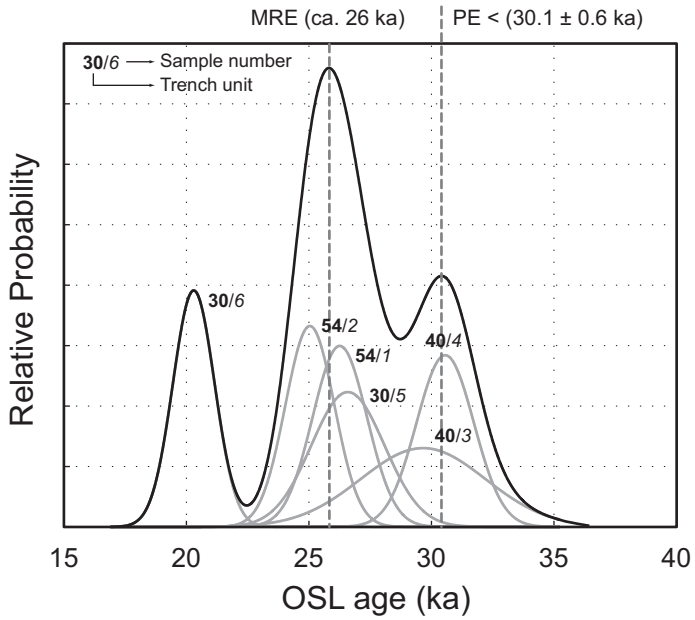

Figure 9. The total results of OSL analyses are presented as individual normal distributions (gray lines) and summed to produce a composite curve (black line). Bold numbers correspond to the sampled unit, and the numbers in italics refer to sample number in Table 1.

11. SUPPLEMENTARY MATERIALS

Table S1. Procedural steps for Single Aliquot Regeneration Protocol for Optical Data.

Table S2. Luminescence Parameters used in Preparation and Analyses of Samples for Quartz OSL.

Figures S1 to S6. Radial plots for each analyzed OSL Sample.

Figure S7. Plot of A) OSL decay and B) growth curve for sample SFT1-6.

Plate S1. Detailed interpretive log for trench T1 presented at the original logged scale.

Plate S2. Detailed interpretive log for test pit TP1 presented at the original logged scale.

Table S1. Single Aliquot Regeneration Protocol for Optical Dating.

1. Preheat (200-240 °C) for 10 seconds (preheat range is specific to Cyprus samples)
2. OSL stimulation with blue light (470 nm) at 125 °C for 40 seconds (L_n)
3. Test dose beta irradiation
4. Cut heat (same temp as preheat) for 0 sec
5. OSL stimulation with blue light (470 nm) at 125 °C for 40 seconds (T_n)
6. Beta irradiation of regeneration dose
7. Preheat (200-240 °C) for 10 seconds
8. OSL stimulation with blue light (470 nm) at 125 °C for 40 seconds (L_x)
9. Test dose beta irradiation
10. Cut heat (same temp as preheat) for 0 sec
11. OSL stimulation with blue light (470 nm) at 125 °C for 40 seconds (T_x)
12. Repeat Steps 6-11 with further regeneration doses

Table S2. Luminescence parameters used in preparation and analyses of samples for quartz OSL

Measurement parameters:	
Machine	Automated Risø TL/luminescence-DA-15
Mineral; grain size:	quartz: 250-180 □m or 180-90 □m
Stimulation source:	blue LED diodes, emission centered on 470 nm
Power delivered to aliquot:	13 mW/cm^2 (90% power)
Duration of stimulation:	40 seconds
Final signal level:	1% of initial
Photomultiplier:	Thorn-EMI 9235Q
Aliquot temperature:	125 °C
Detection filters:	two Hoya U340 filters
Normalization:	none
Preheat:	220 °C (samples <5 ka) for 10 secs
Delay before measurement:	120 sec
Equivalent dose evaluation:	single aliquot regeneration (Murray and Wintle, 2000)
Background evaluation:	black body counts <40 ct/sec, BG counts <45 ct/sec
Alpha effectiveness:	n/a
Dose-rate evaluation:	lab gamma spectrometer (high resolution Ge),
Dose rate range:	1.64-3.67 Gy/ka (average ~2.25 Gy/ka)
Water content:	10-25%
Cosmic-ray contribution:	40% of total dose rate for some near surface samples, 20- 30% average

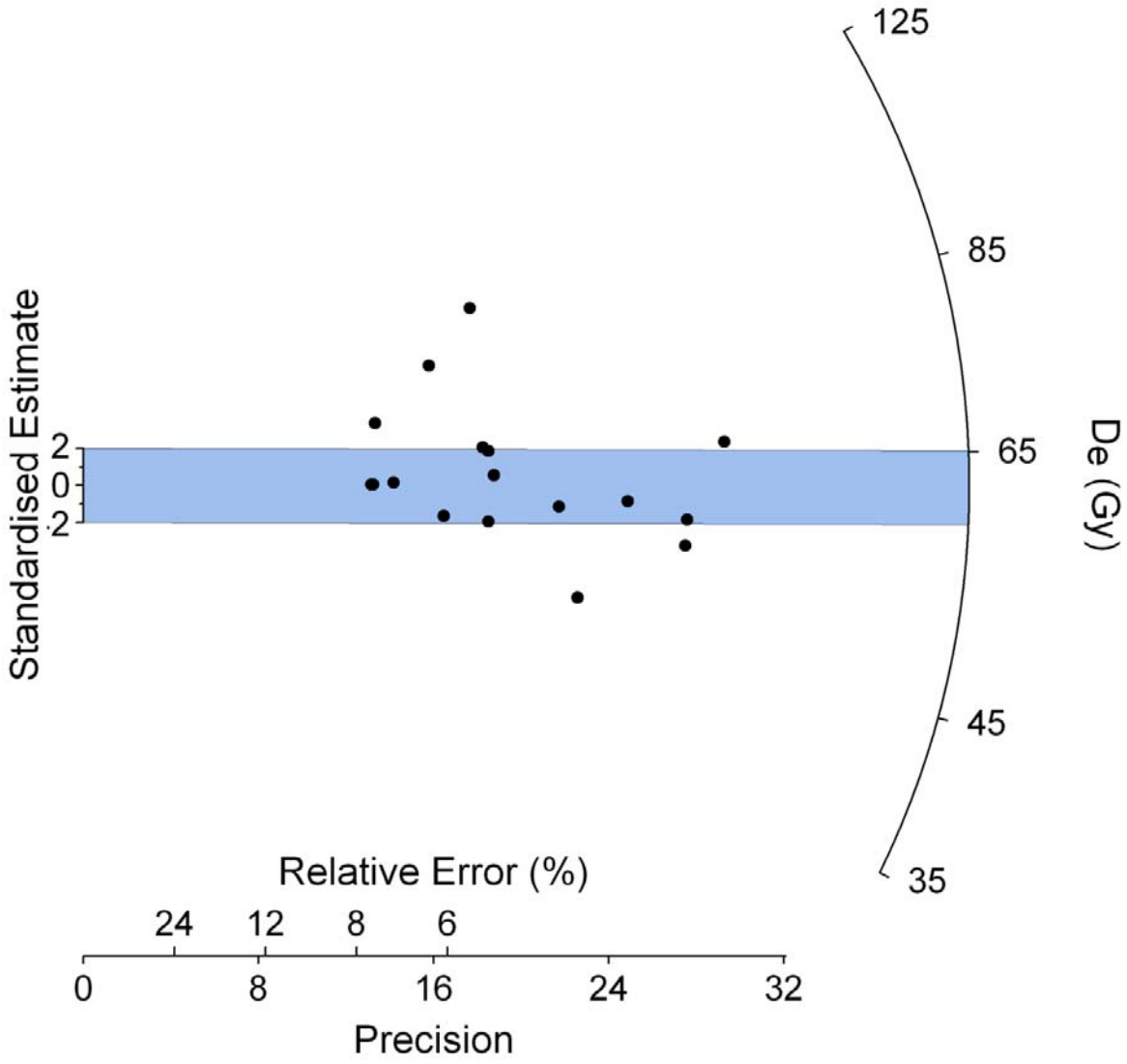

Figure S1. Sample SFTP1-1 showing 17 of 20 aliquots

This sample produced an equal spread of aliquots that plot both above and below the standardized estimate (blue). It is possible that more analyses (i.e., a greater number of aliquots) would resolve a trend within the observed scatter, but for this data the average of the equivalent doses is around 60 Gy, with 18% overdispersion (3/17).

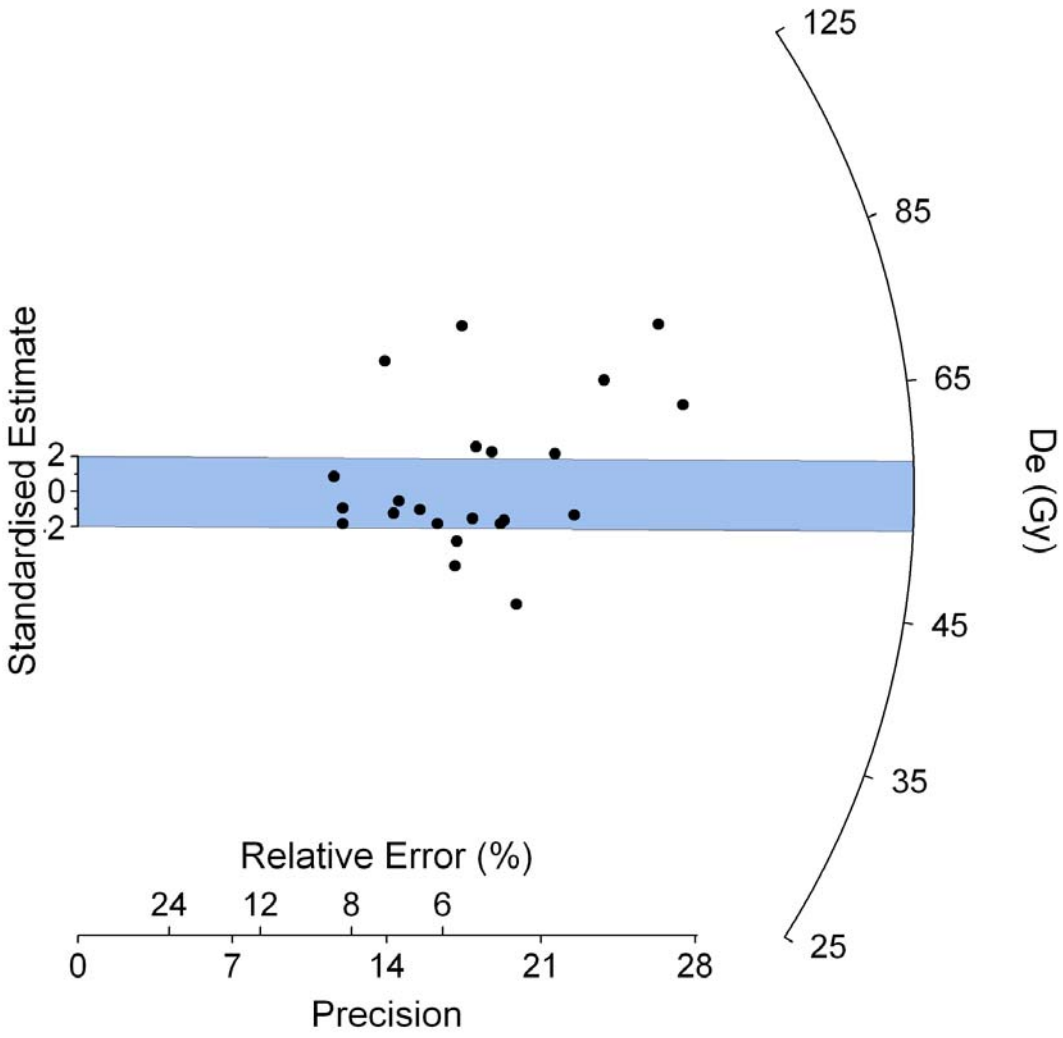

Figure S2. Sample SFTP1-2 showing 22 of 25 aliquots

This sample produced a significant number of aliquots carrying a larger equivalent dose (above the two sigma zone) with varying degrees of precision. Five aliquots plot far above the two sigma standardized estimate (shown in blue) while three aliquots are close to the two sigma estimate (22% over-dispersion, 5/22). The five upper points indicate that grains in these aliquots were not fully bleached prior to deposition, though lower equivalent doses are also common and may indicate bioturbation or sediment mixing.

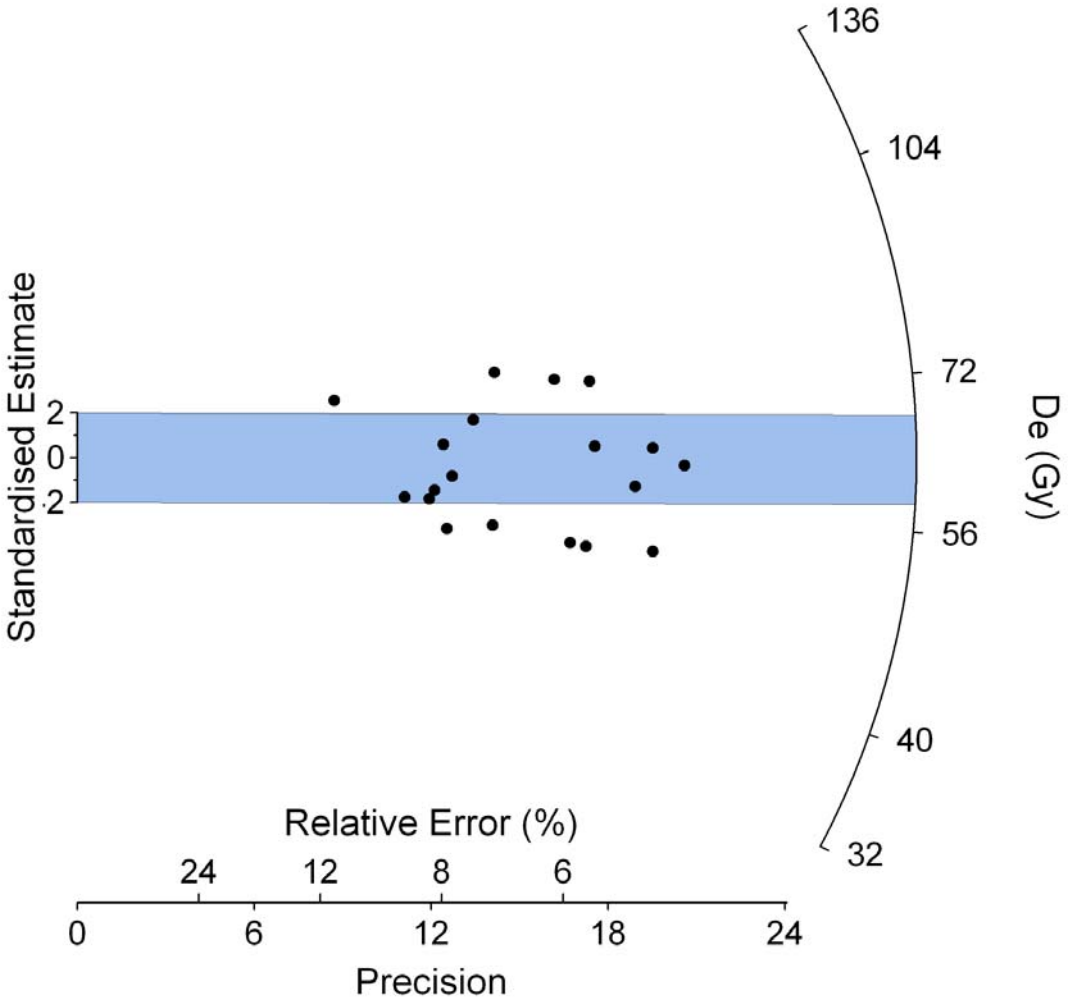

Figure S3. Sample SFTP1-3 showing 17 of 20 aliquots

This plot shows the best bleaching scenario in this set of samples—outlying data points are not systematically high or low, although there is a scatter in the aliquot equivalent dose. The two sigma estimate (in blue) is averaged at about 63 Gy, which is very close to the weighted mean of 66 Gy shown in Table 1.

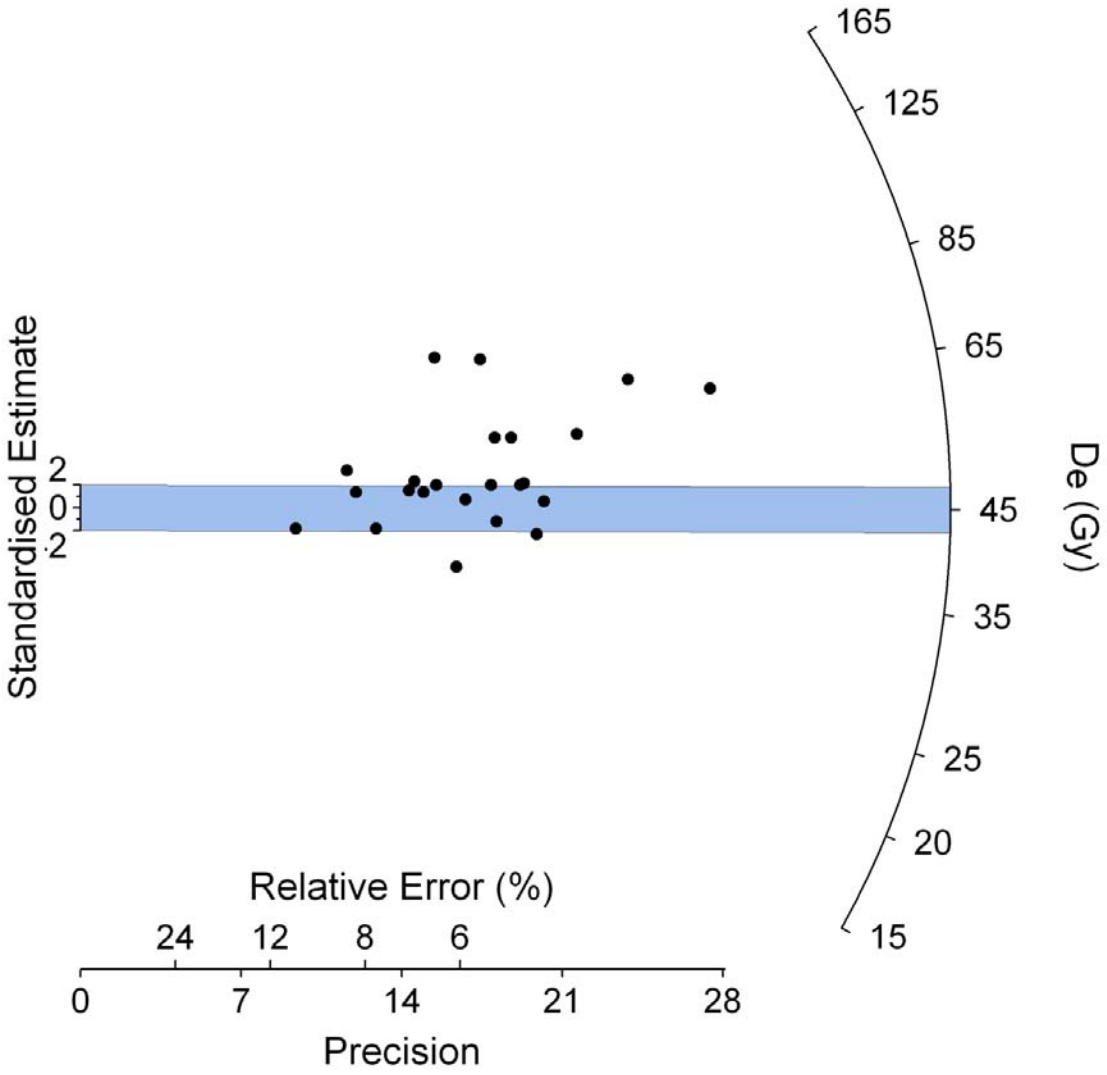

Figure S4. Sample SFTP1-4 showing 23 of 25 aliquots

Several aliquots in this sample carry larger equivalent doses, indicating that this deposit has significant partial bleaching problems compared to samples SFTP1-5 and SFTP1-6. Eight aliquots plot above the two sigma standardized estimate (shown in blue) and indicate that grains in these aliquots were not fully bleached prior to deposition. The over-dispersion of the outliers is about 35% (8/23, discounting the lower outlier), indicating that partial bleaching is a significant factor in the scatter of the equivalent doses.

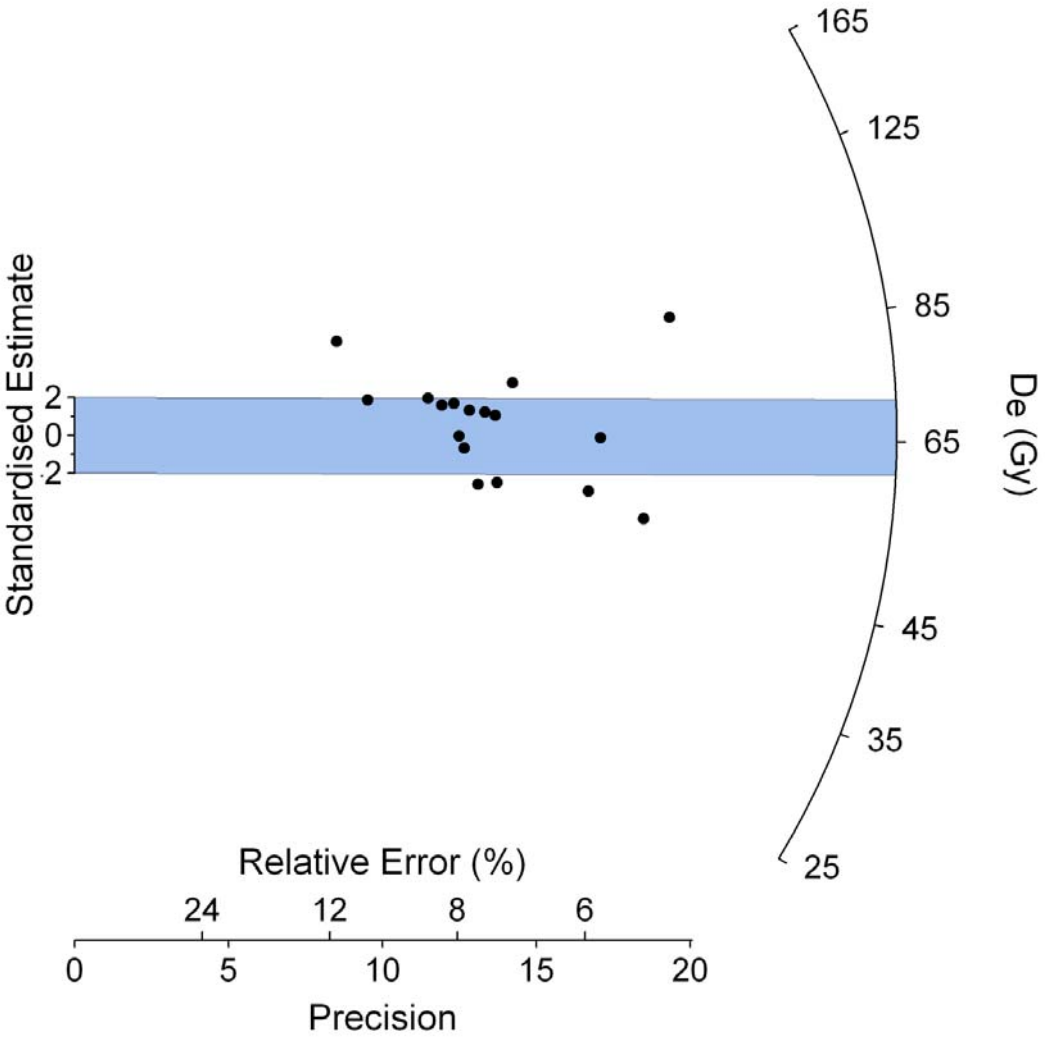

Figure S5. Sample SFTP1-5 showing 17 of 20 aliquots. As in sample SFTP1-6, two notable outliers shows larger equivalent doses. One is more precise (90.8 ± 4.7 Gy with a 5% relative error) and one is less precise (118 ± 14 Gy with a 12% relative error). Both points plot above the two sigma standardized estimate (shown in blue) and indicate that grains in these aliquots were not fully bleached prior to deposition. The over-dispersion of the outliers is about 18% (3/17), indicating that partial bleaching may be a factor in the scatter of the equivalent doses, though lower equivalent doses are also common and may indicate bioturbation or sediment mixing.

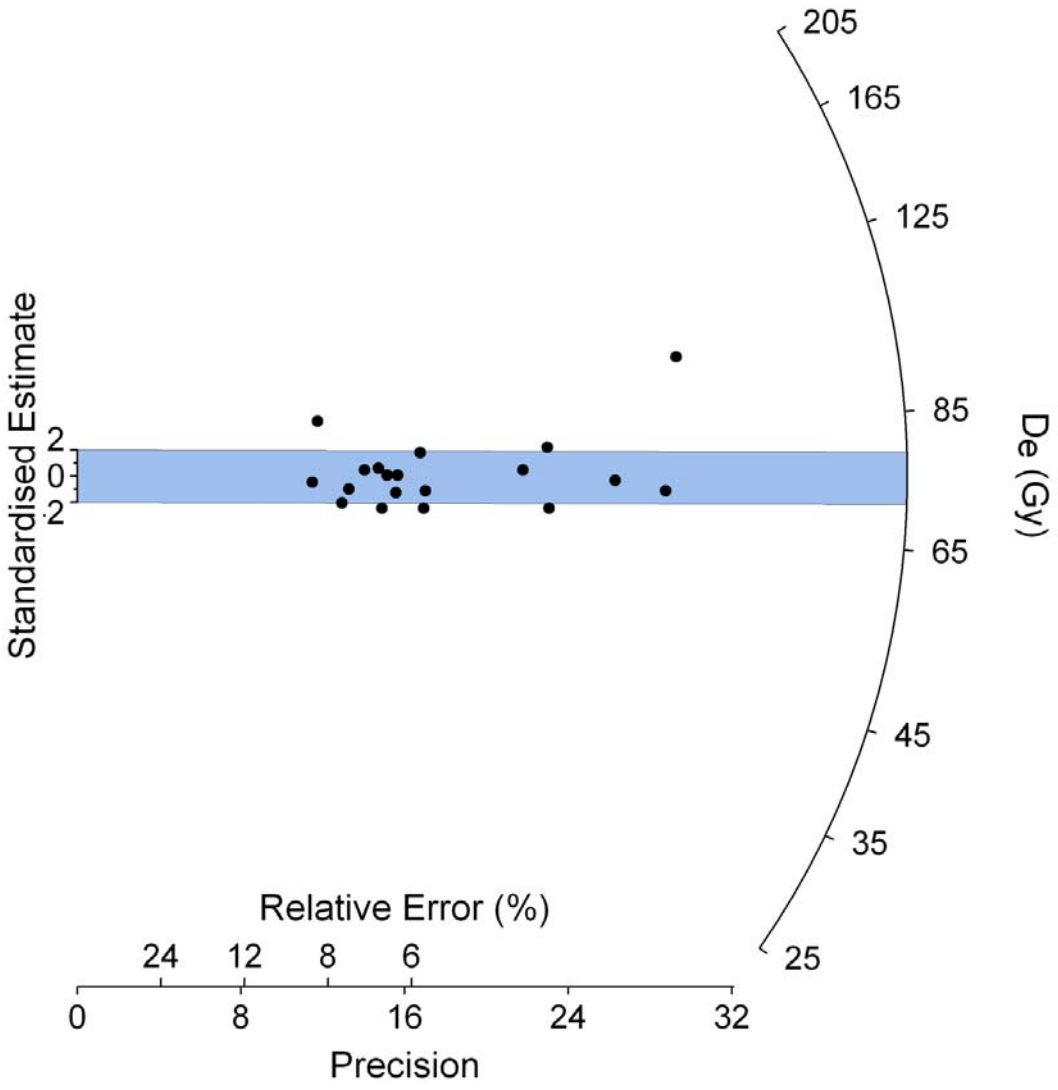

Figure S6. Sample SFTP1-6 showing 19 of 20 aliquots

Two notable outliers in sample SFTP1-6 show larger equivalent doses—one is very precise (103 ± 3.5 Gy with a relative error of 3%) and one is less precise (107 ± 9.1 Gy with a relative error of 8.5%). The more precise point plots near the De (Gy) axis furthest above the two sigma standardized estimate (shown in blue) and indicates that grains in this aliquot were not fully bleached prior to deposition. The over-dispersion of the outliers is about 11% (2/19), indicating that partial bleaching is not a significant factor in the scatter of the equivalent doses.

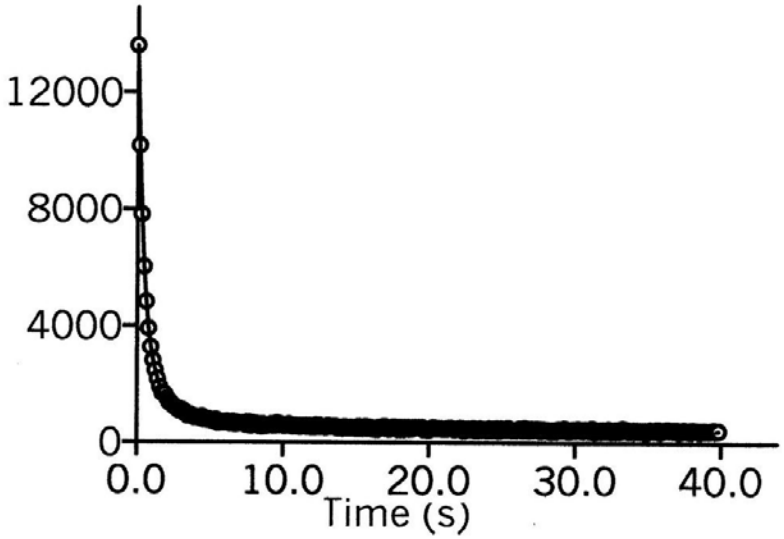

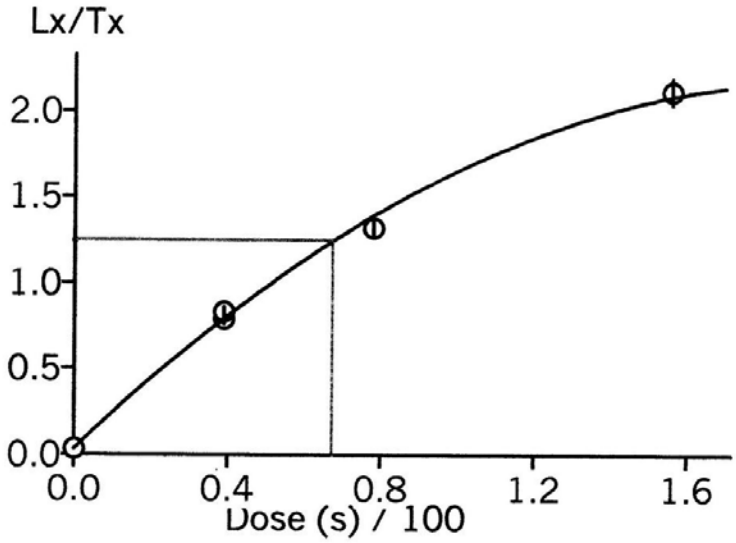

Figure S7. A) Plot of OSL decay curve for SFTP1-6, showing quartz signal accessing the "fast component of OSL". Time is measured in seconds (s) and OSL is measured in photon counts/second and peaked at 13,500 photons/second. B) Plot of SFTP1-6 growth curve—regeneration proceeded "normally," with a recycle within 5% of the first measurement and increases in responses to increasing beta radiation. The beta source delivered ~ 0.071 Gy/s to these coarse-grains mounted on stainless steel discs (at 400 seconds, 800 seconds and1600 seconds). A dose-response curve is fitted through the points and the intercept of the L_N/T_N value is used to obtain a D_e value (in seconds, and hence then in Gy) for the aliquot. The aliquot response is fitted to an exponential curve.

REFERENCES:

Murray, A.S. and Wintle, A.G., 2000, Luminescence dating of quartz using an improved single-aliquot regenerative- dose protocol. Radiation Measurements 32, 57-73.

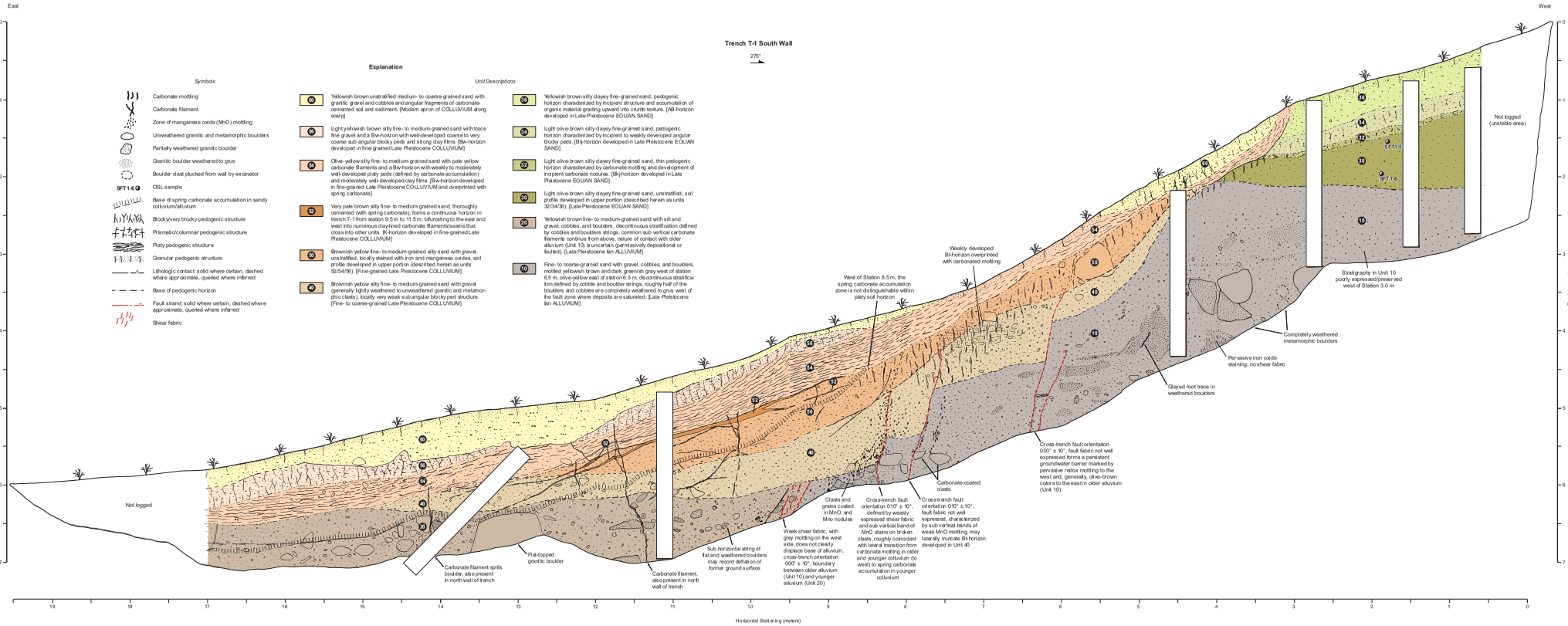
East
West
Trench T-1 South Wall
275°
Explanation
Symbols
Carbonate mottling
Carbonate filament
Zone of manganese oxide (MnO) mottling
Unweathered granitic and metamorphic boulders
Partially weathered granitic boulder
Granitic boulder weathered to grus
Boulder dast plucked from wall by excavator
SFT1-6 OSL sample
Base of spring carbonate accumulation in sandy colluvium/alluvium
Blocky/very blocky pedogenic structure
Prismatic/columnar pedogenic structure
Platy pedogenic structure
Granular pedogenic structure
Lithologic contact: solid where certain, dashed where approximate, queried where inferred
Base of pedogenic horizon
Fault strand: solid where certain, dashed where approximate, queried where inferred
Shear fabric
Unit Descriptions
Yellowish brown unstratified medium- to coarse-grained sand with granitic gravel and cobbles and angular fragments of carbonate-cemented soil and sediment. [Modern apron of COLLUVIUM along scarp]
Light yellowish brown silty fine- to medium-grained sand with trace fine gravel and a Bw-horizon with well-developed coarse to very coarse sub angular blocky peds and strong clay films. [Bw-horizon developed in fine-grained Late Pleistocene COLLUVIUM]
Olive-yellow silty fine- to medium-grained sand with pale yellow carbonate filaments and a Bw-horizon with weakly to moderately well-developed platy peds (defined by carbonate accumulation) and moderately well-developed clay films. [Bw-horizon developed in fine-grained Late Pleistocene COLLUVIUM and overprinted with spring carbonate]
Very pale brown silty fine- to medium-grained sand, thoroughly cemented (with spring carbonate), forms a continuous horizon in trench T-1 from station 9.5 m to 11.5 m, bifurcating to the east and west into numerous clay-lined carbonate filaments/seams that cross into other units. [K-horizon developed in fine-grained Late Pleistocene COLLUVIUM]
Brownish yellow fine- to medium-grained silty sand with gravel, unstratified, locally stained with iron and manganese oxides, soil profile developed in upper portion (described herein as units 52/54/56). [Fine-grained Late Pleistocene COLLUVIUM]
Brownish yellow silty fine- to medium-grained sand with gravel (generally lightly weathered to unweathered granitic and metamorphic clasts), locally very weak sub angular blocky ped structure. [Fine- to coarse-grained Late Pleistocene COLLUVIUM]
Yellowish brown silty clayey fine-grained sand, pedogenic horizon characterized by incipient structure and accumulation of organic material grading upward into crumb texture. [AB-horizon developed in Late Pleistocene EOLIAN SAND]
Light olive-brown silty clayey fine-grained sand, pedogenic horizon characterized by incipient to weakly developed angular blocky peds. [Bt-horizon developed in Late Pleistocene EOLIAN SAND]
Light olive-brown silty clayey fine-grained sand, thin pedogenic horizon characterized by carbonate mottling and development of incipient carbonate nodules. [Bk-horizon developed in Late Pleistocene EOLIAN SAND]
Light olive-brown silty clayey fine-grained sand, unstratified, soil profile developed in upper portion (described herein as units 32/34/36). [Late Pleistocene EOLIAN SAND]
Yellowish brown fine- to medium-grained sand with silt and gravel, cobbles, and boulders, discontinuous stratification defined by cobbles and boulders strings, common sub vertical carbonate filaments continue from above, nature of contact with older alluvium (Unit 10) is uncertain (permissively depositional or faulted). [Late Pleistocene Ian ALLUVIUM]
Fine- to coarse-grained sand with gravel, cobbles, and boulders, mottled yellowish brown and dark greenish gray west of station 6.5 m, olive-yellow east of station 6.5 m, discontinuous stratification defined by cobble and boulder strings, roughly half of the boulders and cobbles are completely weathered to grus west of the fault zone where deposits are saturated. Late Pleistocene Ian ALLUVIUM]
Not logged
Carbonate filament splits boulder, also present in north wall of trench
Flat-topped granitic boulder
Carbonate filament, also present in north wall of trench
Sub horizontal string of fat and weathered boulders may record deflation of former ground surface
Clasts and grains coated in MnO2 and Mno nodules
Weak shear fabric, with grey mottling on the west side, does not clearly displace base of alluvium, cross-trench orientation 000° ± 10°, boundary between older alluvium (Unit 10) and younger alluvium (Unit 20)
Cross-trench fault orientation 010° ± 10°, defined by weakly expressed shear fabric and sub vertical band of MnO stains on broken clasts, roughly coincident with lateral transition from carbonate mottling in older and younger colluvium (to west) to spring carbonate accumulation in younger colluvium
Carbonate-coated clasts
Cross-trench fault orientation 010° ± 10°, fault fabric not well expressed, characterized by sub vertical bands of weak MnO mottling, may laterally truncate Bt-horizon developed in Unit 40
West of Station 8.5 m, the spring carbonate accumulation zone is not distinguishable within platy soil horizon
Weakly developed Bt-horizon overprinted with carbonated mottling
Cross-trench fault orientation 030° ± 10°, fault fabric not well expressed forms a persistent groundwater barrier marked by pervasive redox mottling to the west and, generally, olive-brown colors to the east in older alluvium (Unit 10)
Gleyed root trace in weathered boulders
Pervasive iron oxide staining; no shear fabric
Completely weathered metamorphic boulders
Stratigraphy in Unit 10 poorly expressed/preserved west of Station 3.0 m
Not logged (unstable area)
SFT1-5
SFT1-6
Depth (meters)
Horizontal Stationing (meters)

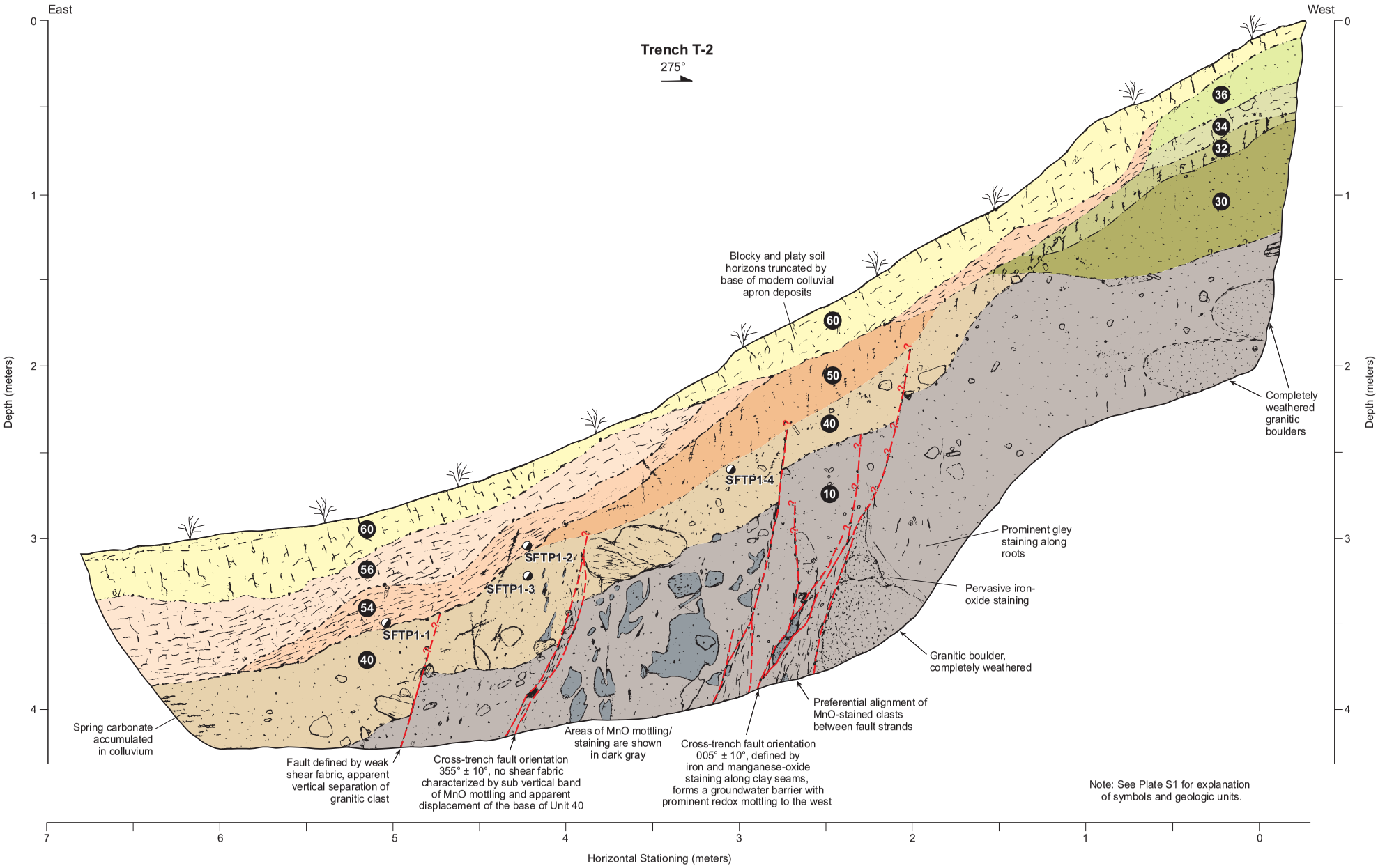
East
West
Trench T-2
275°
Depth (meters)
Horizontal Stationing (meters)
0
1
2
3
4
7
6
5
4
3
2
1
0
36
34
32
30
60
50
40
10
60
56
54
40
SFTP1-1
SFTP1-2
SFTP1-3
SFTP1-4
Blocky and platy soil horizons truncated by base of modern colluvial apron deposits
Completely weathered granitic boulders
Prominent gley staining along roots
Pervasive iron-oxide staining
Granitic boulder, completely weathered
Preferential alignment of MnO-stained clasts between fault strands
Spring carbonate accumulated in colluvium
Fault defined by weak shear fabric, apparent vertical separation of granitic clast
Cross-trench fault orientation 355° ± 10°, no shear fabric characterized by sub vertical band of MnO mottling and apparent displacement of the base of Unit 40
Areas of MnO mottling/ staining are shown in dark gray
Cross-trench fault orientation 005° ± 10°, defined by iron and manganese-oxide staining along clay seams, forms a groundwater barrier with prominent redox mottling to the west
Note: See Plate S1 for explanation of symbols and geologic units.